https://doi.org/10.5194/essd-2026-213
Preprint. Discussion started: 18 May 2026


Open Access Earth System Science Data Discussions

# Alaska-COLD: Linking Surface Temperatures and Subsurface Thermal Dynamics in a Multi-Year Hourly Dataset From Interior and Northern Alaska

Aymane Ahajjam [1], Anaí Caparó Bellido [2], Andrew Wilcox [2], Mary Soaper [3], Hayden Patterson [3], Sydney Weaver [3], Shishay Kidanu[3], and Timothy Pasch [4]

[1]School of Electrical Engineering and Computer Science, University of North Dakota, Grand Forks, ND, USA
[2]Department of Earth System Science & Policy, University of North Dakota, Grand Forks, ND, USA
[3]Harold Hamm School of Geology & Geological Engineering, University of North Dakota, Grand Forks, ND, USA
[4]Department of Communication, University of North Dakota, Grand Forks, ND, USA

**Correspondence:** Timothy Pasch (timothy.pasch@und.edu)

**Abstract.** We present the Alaska Coupled Observations of Land-atmosphere Dynamics (Alaska-COLD) dataset, comprising hourly air and soil temperature measurements from 12 sites across Alaska's north-central regions (64°-70°N). Each site measures air temperature and soil temperatures at four depths (0-0.7 m). Seven sites provide 714-726 days of continuous records (Summer 2023-2025) capturing multiple freeze-thaw (FT) cycles. We classify FT phenology into thawing, thawed, freezing, and frozen phases using surface temperature observations, enabling phase-specific analysis of thermal dynamics. We further derive FT metrics, including $n$-factors, degree-day totals, and damping ratios, to characterize surface energy exchange and subsurface thermal attenuation. The records reveal strong thermal damping with depth: surface-soil diurnal amplitudes range from 0.7-4.3°C, while the deepest sensors show only 0.004-0.047°C variation across the mean daily cycle. At the annual scale, ground-temperature ranges decrease from 11-25°C near the surface to 3-5°C at 45-75 cm depth, compared with air-temperature ranges of 36-45°C. Thawed periods range from 39 to 92 days annually, and air-ground coupling vary strongly by FT phase, with $R^2$ increasing from 0.02 during thawing to 0.69 during thawed conditions. A concise comparison with co-located ERA5-Land estimates shows stronger agreement for air temperature than for soil temperatures, highlighting the value of Alaska-COLD for resolving site-level ground thermal dynamics in permafrost environments. Alaska-COLD is accessible via: https://doi.org/10.5281/zenodo.17980271.

## 1 Introduction

The Arctic is among the most sensitive regions, where rapid atmospheric shifts can drive permafrost thaw that destabilizes previously frozen ground and triggers ground subsidence, slope collapse, and thermokarst formation, threatening critical transportation and energy infrastructure Park et al. (2016); Cohen et al. (2014); Hjort et al. (2022); Rantanen et al. (2022). Alaska exemplifies the risks of permafrost thaw, putting billions of dollars of infrastructure at risk if thawing continues Romanovsky et al. (2010b); Manos et al. (2025); Walsh and Brettschneider (2019). Because permafrost thaw is governed by interactions between surface weather and subsurface heat transfer Smith et al. (2022); Kurylyk et al. (2016), understanding and anticipat-

https://doi.org/10.5194/essd-2026-213
Preprint. Discussion started: 18 May 2026


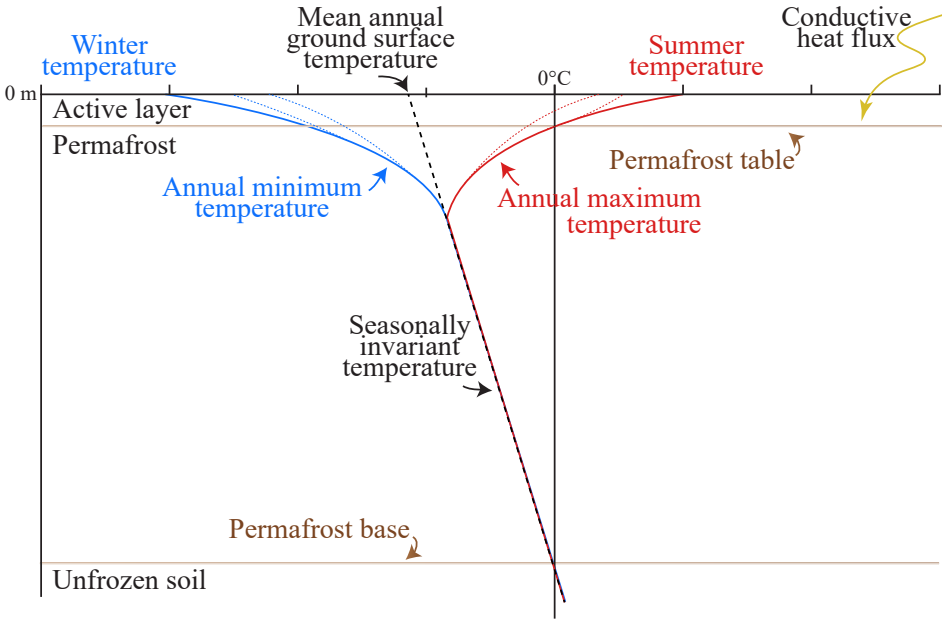


**Figure 1.** Conceptual schematic of the vertical ground temperature structure in permafrost terrain illustrating the penetration of surface thermal variability with depth. Seasonal extremes in ground temperature are shown by typical winter (blue) and summer (red) profiles, defining the annual minimum and maximum temperature envelopes within the active layer. The mean annual ground surface temperature sets the surface thermal boundary condition, while the zero-degree isotherm and the permafrost table delineate the base of the seasonally thawed layer. With increasing depth, the influence of seasonal forcing diminishes, leading to a seasonally invariant temperature regime controlled primarily by conductive heat flux and the geothermal gradient.

ing impacts requires sustained, high-quality observations of meteorological changes and subsurface thermal regimes across spatially distributed sites.

Permafrost thaw is fundamentally a heat transfer problem, governed by conductive heat fluxes from the ground surface into the subsurface and their interaction with soil thermal properties (see Fig. 1). On seasonal to decadal timescales, thaw progression is driven by changes in ground surface temperature boundary conditions, while ice-rich soils strongly moderate shifting thermal conditions through latent heat consumption during phase change (Putkonen, 1998). Snow cover, vegetation structure, soil texture, and moisture content further modify thermal conductivity and surface energy exchange, resulting in pronounced spatial variability in thaw depth and rates even under similar atmospheric changes (Smith et al., 2022). Consequently, permafrost responses cannot be inferred from air temperature alone and requires direct observation of ground thermal conditions.

The foundation of modern permafrost monitoring rests on international networks that standardized data collection protocols (see Table 1 for a summary of related works). For instance, the Circumpolar Active Layer Monitoring (CALM) program, established in 1991, is the first initiative to provide a shared database of active-layer thickness (ALT) and near-surface temperatures

https://doi.org/10.5194/essd-2026-213
Preprint. Discussion started: 18 May 2026


Open Access Earth System Science Data Discussions

**Table 1.** Summary of Related Permafrost and Meteorological Dataset Papers.

| Reference (year) | Region | Approach | Variables | Period / Res. |
|---|---|---|---|---|
| **Swanson et al. (2021)** | *Alaska* | 33 NPS weather stations and 8 NWS stations across northernmost national parks | MAAT, MAGT | 2014-2019 / Annual |
| **Wang et al. (2018)** | *Alaska* | Data harmonization from 72 USGS, NPS, and UAF stations | Air/Soil temperatures (<1m), soil moisture, snow depth | 1997-2016 / Monthly |
| **Urban and Clow (2018)** | *Alaska (NPR-A and ANWR)* | 16-station DOI/GTN-P monitoring arrays across geomorphic and vegetation gradients | Soil temperatures (5-120cm), ALT, soil moisture, meteorological parameters | 1998-2019 / Hourly |
| **Biskaborn et al. (2015)** | *Global* | Centralized database integrating TSP boreholes and CALM sites | Soil temperatures, ALT | 1990s-ongoing / Varies by site |
| **Clow (2014)** | *Alaska* | 23-element DOI/GTN-P deep borehole array with calibrated, deconvolved temperature logs | Soil temperatures | 1973-2013 / Varies by site |
| **Romanovsky et al. (2010b)** | *Northern Hemisphere* | Enhanced monitoring network for IPY: 570+ boreholes across North America, Nordic region, and Russia | MAGT, Soil temperatures | 1970s-2009 / Varies by site |
| **Osterkamp (2005)** | *Alaska* | Long-term borehole network with temperature loggers at 11 levels | Air/Soil temperatures (<1m), ALT | 1977-2004 / Hourly |
| **Brown et al. (2000)** | *Circumpolar Arctic* | Documentation of CALM network: 100+ sites across 15 countries | near-surface Soil temperatures, ALT | 1991-ongoing / Annual |
| **Romanovsky and Osterkamp (1995)** | *Prudhoe Bay, Alaska* | Transect measurements with sensors at multiple depths | Air/Soil temperatures (<1m) | 1986-1992 / 4-hourly |
| **This Study (2026)** | *Alaska* | 12-station network with multi-depth thermistors. | Air/Soil temperatures (0–0.7 m), and meteorological parameters | 2023-ongoing / Hourly |

across 15 countries (Brown et al., 2000). In 1999, the Global Terrestrial Network for Permafrost (GTN-P) was established under the World Meteorological Organization's GCOS initiative in collaboration with the International Permafrost Association (IPA). The network integrates active layer thickness (ALT) observations from the CALM program with measurements of the thermal state of permafrost (TSP) obtained from an extensive borehole network (Romanovsky et al., 2010b; Streletskiy et al., 2020). This monitoring network was substantially expanded by the International Polar Year Thermal State of Permafrost (IPY TSP) project, which increased global borehole coverage (Romanovsky et al., 2010a) and produced a snapshot of per-

https://doi.org/10.5194/essd-2026-213
Preprint. Discussion started: 18 May 2026




mafrost conditions during the 2007–2009 International Polar Year. These efforts were subsequently consolidated within the new GTN-P database by Biskaborn et al. (2015). More recent assessments emphasize that the coordinated GTN-P monitoring framework is critical for international weather pattern assessments and process understanding (e.g., IPCC, SWIPA), while remaining dependent on sustained observational infrastructure (Streletskiy et al., 2020).

In Alaska, long-term thermal records have been instrumental in documenting the statewide responses to weather parameter forcing. Osterkamp (2005) utilized a borehole network established in 1977 to trace shifting thermal trends across decades, demonstrating a clear correlation between air temperatures changes and subsurface thermal degradation. To address the challenge of data fragmentation across various agencies, Wang et al. (2018) developed the PF-AK v0.1 dataset. This effort harmonized data from 72 stations, including sites from the U.S. Geological Survey, National Park Services, and the University of Alaska Fairbanks Geophysical Institute. PF-AK provides monthly ground temperatures at depths up to 1m, volumetric soil water content, snow depth, and air temperature covering the period 1997 to 2016. Complementing these records, Swanson et al. (2021) analyzed ground and weather monitoring data across Alaska's northernmost national parks, demonstrating how recent increases in MAATs have accelerated permafrost degradation across both Arctic and sub-Arctic landscapes.

While broad networks provide regional trends, localized monitoring efforts are also necessary to capture the fine-scale physics of thaw. Early efforts at Prudhoe Bay, AK by Romanovsky and Osterkamp (1995) established the utility of permafrost monitoring at sub-daily temporal resolutions (4–6 h sampling intervals) for capturing interannual variations in the active layer and near-surface permafrost from weather variations. On the Arctic Slope, Clow (2014) assembled and analyzed subsurface temperature profiles from a set of 23 deep boreholes (∼500–800 m). These boreholes were originally drilled during U.S. Department of the Interior oil exploration programs at different times over the period 1973–2013. More recently, Urban and Clow (2018) deployed 16 monitoring stations across the National Petroleum Reserve–Alaska (NPR-A) and Arctic National Wildlife Refuge (ANWR). At hourly resolution, the stations monitor shallow permafrost temperatures (5–120 cm), active layer thickness, soil moisture, as well as meteorological variables. The dataset spans the period from 1998 to 2019 and has contributed to several international monitoring frameworks, including GTN-P, GCOS, and CALM.

Nevertheless, the current state of Arctic permafrost monitoring presents several persistent limitations. Many monitoring stations have ceased operation, primarily due to reliance on short-term research funding and voluntary contributions, but also the harsh environmental conditions that complicate all monitoring aspects, including long-term operation (Streletskiy et al., 2020). In addition, most existing networks operate at relatively coarse temporal resolution, limiting their utility for addressing short-term variability and their use in data-intensive approaches (e.g., machine learning). Moreover, the ongoing monitoring efforts provide limited coverage across the diversity of permafrost landscapes, ground-ice conditions, and land cover types, constraining their applicability to regional-scale assessments. These limitations motivate the development of complementary permafrost monitoring approaches that improve temporal resolution, continuity, and environmental representativeness, particularly in Alaska.

The Defense Resiliency Platform Against Extreme Cold Weather (DRP) was established in 2022 as an interdisciplinary research initiative funded by the U.S. Army Corps of Engineers to support understanding and prediction of infrastructure vulnerability under extreme cold conditions (U.S. Army Corps of Engineers Cold Regions Research and Engineering Laboratory,

https://doi.org/10.5194/essd-2026-213
Preprint. Discussion started: 18 May 2026




2024). Led by Virginia Tech in collaboration with multiple academic and federal partners, the DRP develops integrated cyberinfrastructure to support data-driven assessment and prediction of cold-region environmental and infrastructure processes (Pasch and UND ARCTIC Lab, 2024).

Data acquisition within the DRP spans multiple observational modalities, including airborne and terrestrial LiDAR (Pasch et al., 2023a, b, c, d, e, f, g, h, i, j; Chukwuemeka et al., 2025b, d, e, c, 2024b, c, 2025a), multispectral and electro-optical imagery (Chukwuemeka et al., 2022a, 2023; Chukwuemeka, 2024), and field-based meteorological and geophysical measurements collected using aerial, vehicle-mounted, and ground-based platforms across Alaska (Chukwuemeka et al., 2022b, 2024a). All datasets are curated and integrated within the DRP cyberinfrastructure platform (https://drp.dataone.org/), enabling cross-modal analysis and predictive modeling.

The Alaska-COLD dataset presented in this paper represents the ground-based thermal monitoring component of the DRP. It provides hourly air and ground temperature observations across a 64°–70°N latitudinal transect, spanning discontinuous to continuous permafrost zones and a range of dominant ecotypes along the Dalton Highway corridor. These observations support the characterization of air–ground thermal coupling and enable upscaling of in situ measurements for environmental modeling applications (Cable et al., 2016). In addition, a freeze–thaw phenological framework is applied to partition the annual thermal cycle into thawing, thawed, freezing, and frozen phases, allowing phase-specific analysis of thermal damping and subsurface response.

The remainder of this paper is organized as follows. Section 2 describes the study region, criteria for site selection, and environmental characteristics of each site. In addition, it details the instrumentation, data acquisition procedures, and processing methods used to generate the dataset. Section 3 explains how surface Freeze-Thaw (FT) phenology phases are defined as well as the derived variables. Sections 4 and 5 present and discuss the dataset evaluation, including spatial and temporal patterns across the monitoring network and a concise comparison with co-located ERA5-Land temperature estimates. Finally, Section 6 summarizes the main contributions of this dataset and outlines future research.

## 2 Monitoring Network and Site Characteristics

The monitoring network comprises 12 automated ground and meteorological stations distributed between 65°N and 70°N across northern and interior Alaska. Fig. 2 shows two examples of the monitoring stations under different weather conditions and located in different land covers, while Fig. 3 shows the location of all the 12 sites and their respective names. These sites capture the long-term weather patterns and ecological transition from boreal forest to Arctic tundra, encompassing both discontinuous and continuous permafrost zones where ground-ice content, vegetation type, and snow regimes vary sharply with latitude, elevation, and terrain. All stations were installed on undisturbed terrain representative of surrounding conditions and positioned away from infrastructure or local disturbances.

https://doi.org/10.5194/essd-2026-213
Preprint. Discussion started: 18 May 2026


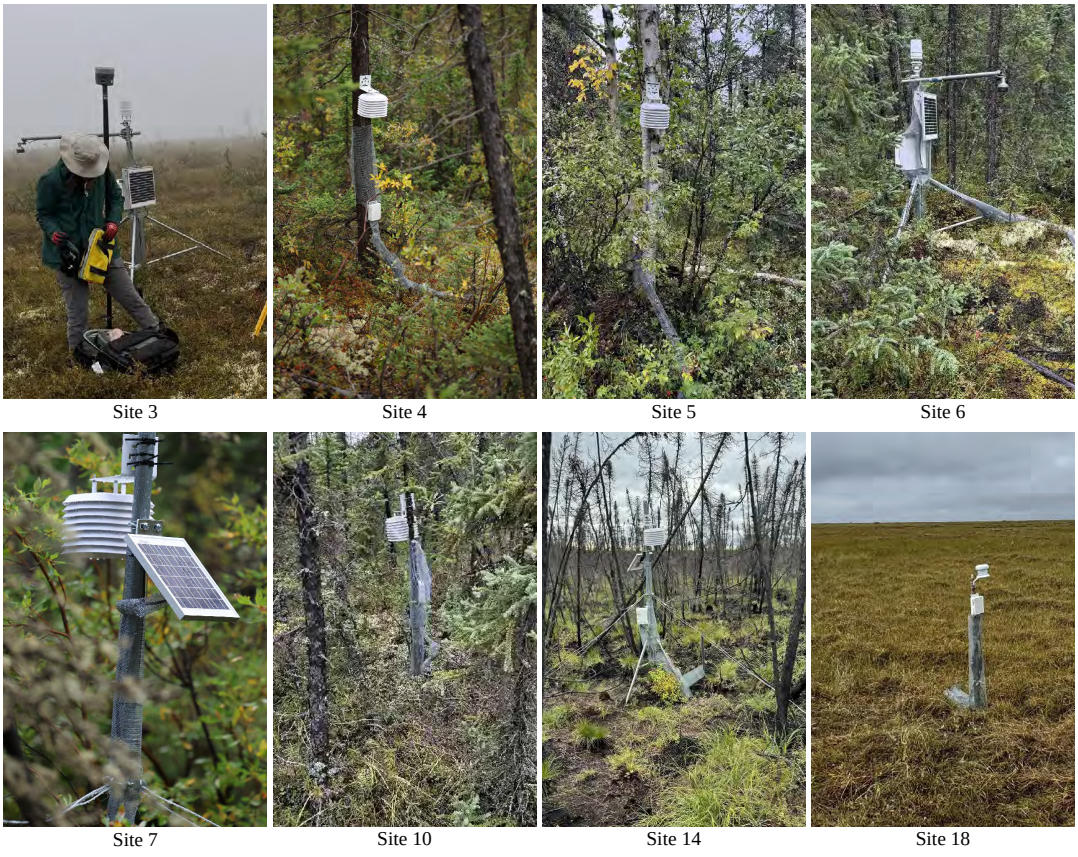


**Figure 2.** Examples of monitoring stations installed at the study sites.

### 2.1 Sites Description

Site elevations range from approximately 140m a.s.l. along the northern coastal plain (North Slope North) to over 700m in the Tanana Highlands. Long-term mean annual air temperature (MAAT) (1994-2024, ERA5-Land) decreases northward from roughly -4.4°C in the boreal forest to about -9.5°C in the Arctic tundra, reflecting the pronounced latitudinal and continental thermal gradients of Alaska's interior–slope corridor. The southern Tanana Highlands and Central Brooks Foothills experience warmer conditions (-2 to -4°C MAAT) and support black and white spruce forests with moss–lichen understories typical of the boreal biome. Northward, the landscape grades into upland shrub tundra around Toolik and Imnavait Creek, where patchy snow accumulation and vegetation height modulate active layer thickness and soil freezing dynamics. Beyond the continental divide, the North Slope lowlands around Prudhoe Bay are underlain by continuous permafrost (MAAT < -8°C) with shallow active layers, polygonal tundra surfaces, and minimal vegetation insulation. These vegetation transitions, ranging from white and black spruce forests with moss–lichen understories in the southern sites to mixed shrub–graminoid tundra and low-centered polygon terrain on the coastal plain, are consistent with regional ecoregions and vegetation classes derived from the Ecoregions

https://doi.org/10.5194/essd-2026-213
Preprint. Discussion started: 18 May 2026


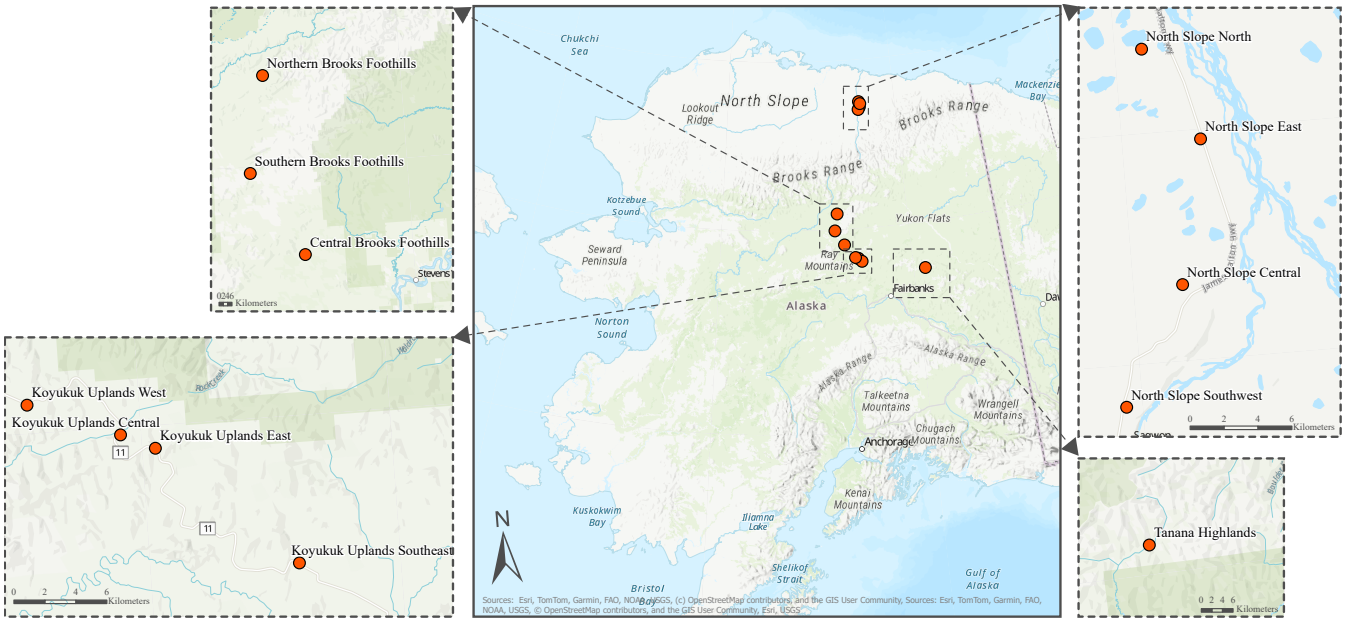


**Figure 3.** Location of monitored sites in Alaska.

of the World and Alaska Vegetation and Wetland Composite datasets. A summary of the characteristics of each site is reported in Tables 2, 3, and 4.

**Table 2.** General characteristics of the monitored sites.

| ID | Site Name | Latitude | Longitude | Elevation (m a.s.l.)[1] | Start - End dates | Soil Depths (cm) (Probe 1, 2, 3, 4) |
|---|---|---|---|---|---|---|
| 3 | Southern Brooks Foothills | 66.488259 | -150.695732 | 610.4 | 05 Aug 2023 - 27 Jul 2025 | 0, 13.9, 29.2, 45.1 |
| 4 | Koyukuk Uplands Central | 65.798635 | -149.4432 | 335.06 | 08 Aug 2023 - 30 Jul 2025 | 0, 12.4, 26.8, 40.9 |
| 5 | Koyukuk Uplands East | 65.789522 | -149.395576 | 496.64 | 09 Aug 2023 - 27 Jul 2025 | 0, 18.7, 39.9, 59.8 |
| 6 | Koyukuk Uplands Southeast | 65.717295 | -149.204995 | 235.96 | 11 Aug 2023 - 30 Jul 2025 | 0, 16.0, 31.9, 48.3 |
| 7 | Koyukuk Uplands West | 65.819491 | -149.571774 | 493.59 | 10 Aug 2023 - 08 May 2024 | 0, 16.7, 33.2, 49.4 |
| 9 | North Slope Central | 69.452173 | -148.638054 | 227.28 | 02 Aug 2023 - 28 Jul 2025 | 0, 8.0, 21.0, 34.0 |
| 10 | Central Brooks Foothills | 66.138147 | -150.173456 | 244.6 | 24 Jul 2024 - 27 Jul 2025 | 0, 24.2, 47.0, 69.8 |
| 11 | Tanana Highlands | 65.417338 | -145.586821 | 706.34 | 12 Aug 2023 - 26 Jul 2025 | 0, 18.9, 37.1, 55.3 |
| 13 | North Slope Southwest | 69.389001 | -148.735198 | 291.92 | 03 Aug 2023 - 28 Jul 2025 | 0, 8.4, 19.6, 31.5 |
| 14 | Northern Brooks Foothills | 66.894138 | -150.515111 | 357.81 | 04 Aug 2023 - 24 Jul 2024 | 0, 24.0, 48.0, 72.0 |
| 15 | North Slope North | 69.579838 | -148.670741 | 145.41 | 11 Jan 2025 - 29 Jul 2025 | 0, 10.5, 23.0, 34.5 |
| 18 | North Slope East | 69.529292 | -148.593929 | 162.18 | 23 Jul 2024 - 28 Jul 2025 | 0, 12.33, 24.67, 37.0 |

https://doi.org/10.5194/essd-2026-213
Preprint. Discussion started: 18 May 2026


Open Access Earth System Science Data Discussions

**Table 3.** Ecological characteristics of the monitored sites. BF = Boreal Forest, WS = White Spruce, BS = Black Spruce, TT = Tussock Tundra, W-O = Woodland-Open, O-C = Open-Closed, LS = Low Shrub, H = Herbaceous.

| ID | Site Name | Permafrost | Cover[1] | Biome[2] | Vegetation[3] | MAAT[4] (°C) | Soil Type[5] |
|---|---|---|---|---|---|---|---|
| 3 | Southern Brooks Foothills | Discontinuous | Tundra | Grassland | LS | -4.80 | Sandy Loam |
| 4 | Koyukuk Uplands Central | Discontinuous | BF/Taiga | Tree cover | Dwarf Shrub-Lichen | -4.53 | Sandy Loam |
| 5 | Koyukuk Uplands East | Discontinuous | BF/Taiga | Tree cover | WS or BS-Deciduous (O-C) | -4.53 | Sandy Loam |
| 6 | Koyukuk Uplands Southeast | Discontinuous | BF/Taiga | Tree cover | WS or BS (O-C) | -4.42 | Loam |
| 7 | Koyukuk Uplands West | Discontinuous | BF/Taiga | Tree cover | WS or BS (Woodland) | -4.44 | Sandy Loam |
| 9 | North Slope Central | Continuous | Tundra | Grassland | TT (LS or H) | -9.33 | Silt Loam |
| 10 | Central Brooks Foothills | Discontinuous | BF/Taiga | Tree cover | WS or BS (O-C) | -4.54 | Loam |
| 11 | Tanana Highlands | Continuous | Tundra | Grassland | Tall Shrub (O-C) | -5.87 | Sandy Loam |
| 13 | North Slope Southwest | Continuous | Tundra | Grassland | LS | -9.50 | Silt Loam |
| 14 | Northern Brooks Foothills | Discontinuous | BF/Taiga | Tree cover | WS or BS/Lichen (W-O) | -5.64 | Sandy Loam |
| 15 | North Slope North | Continuous | Tundra | Moss & lichen | TT (LS or H) | -9.28 | Loam |
| 18 | North Slope East | Continuous | Tundra | Moss & lichen | Dwarf Shrub | -9.33 | Loam |

[1] Based on ESA WorldCover (10 m) (Zanaga et al., 2022).

[2] Ecoregions of the World by Resolve (Dinerstein et al., 2017).

[3] Alaska Vegetation and Wetland Composite (Alaska Center for Conservation Science, 2017).

[4] Mean Annual Air Temperature (MAAT) from ERA5-Land between 1994-2024 (Muñoz Sabater et al., 2021).

[5] Soil type (at 100m depth) based on data from (Hengl, 2018).

## 2.2 Instrumentation Specifications

Hourly measurements of air and soil temperatures are acquired at each site, with two sites measuring additional atmospheric variables. Three datalogger systems are deployed across the network: Campbell Scientific CR350 Campbell Scientific, Inc. (2026a), Onset HOBO H21-USB Onset Computer Corporation (2026a), and Onset HOBO U30 Onset Computer Corporation (2026b), while Campbell and Hobo U30 have their main source of power coming from solar panels, HOBO H21 uses lithium batteries. Table 5 summarizes the sensor specifications for each measurement type.

The CR350 stations (Site 3 and 6) are equipped with Campbell Scientific ClimaVUE 40 compact weather sensors, which provide multiple measurements including air temperature, relative humidity, barometric pressure, vapor pressure, wind speed and direction, precipitation, and lightning activity. The ClimaVUE 40 employs a thermistor mounted on a stainless-steel needle extending from the center of the ultrasonic anemometer assembly. The ClimaVUE 40's temperature sensor is exposed to open air and relies on a firmware-based energy balance correction that accounts for solar loading using concurrent measurements of solar radiation and wind speed. According to manufacturer specifications, this correction yields accuracy equivalent to fan-aspirated shields ($\pm 0.6$°C from $-20$ to 50°C) Campbell Scientific, Inc. (2025). The relative humidity sensor is protected by a Teflon screen that prevents liquid water intrusion while permitting vapor exchange. However, we note that the sensor is not heated, and episodes of rime or frost accumulation during cold, humid conditions may temporarily affect humidity readings Campbell Scientific, Inc. (2025).

https://doi.org/10.5194/essd-2026-213
Preprint. Discussion started: 18 May 2026


Open Access Earth System Science Data Discussions

**Table 4.** Physical properties of the monitored sites.

| ID | Site Name | Excess Ice[1] | Snow density[2] (kg m$^{-3}$) | Snow depth[2] (m) | Surface albedo[2] | Slope[3] (degrees) | Soil bulk density[4] - 100cm[6] (kg m$^{-3}$) |
|---|---|---|---|---|---|---|---|
| 3 | Southern Brooks Foothills | High (>40%) | 170.34 | 0.28 | 0.37 | 0.11 | 13.10 |
| 4 | Koyukuk Uplands Central | High (>40%) | 160.46 | 0.22 | 0.23 | 0.63 | 13.70 |
| 5 | Koyukuk Uplands East | High (>40%) | 160.46 | 0.22 | 0.23 | 0.63 | 13.70 |
| 6 | Koyukuk Uplands Southeast | High (>40%) | 158.34 | 0.21 | 0.23 | 0.62 | 14.30 |
| 7 | Koyukuk Uplands West | High (>40%) | 160.46 | 0.22 | 0.23 | 0.63 | 13.70 |
| 9 | North Slope Central | Moderate (10-40%) | 167.89 | 0.31 | 0.52 | 0.31 | 9.20 |
| 10 | Central Brooks Foothills | Moderate (10-40%) | 166.19 | 0.26 | 0.25 | 1.38 | 13.50 |
| 11 | Tanana Highlands | Moderate (10-40%) | 158.55 | 0.24 | 0.43 | 0.41 | 13.90 |
| 13 | North Slope Southwest | Moderate (10-40%) | 167.84 | 0.31 | 0.52 | 0.30 | 10.40 |
| 14 | Northern Brooks Foothills | Moderate (10-40%) | 177.35 | 0.34 | 0.39 | 0.94 | 12.50 |
| 15 | North Slope North | High (>40%) | 167.39 | 0.28 | 0.50 | 0.15 | 9.40 |
| 18 | North Slope East | Moderate (10-40%) | 167.39 | 0.28 | 0.50 | 0.15 | 9.40 |

[1] Excess ice volume in top 5m (Jorgenson et al., 2008).

[2] Snow density, snow depth, surface albedo from ERA5-Land(Muñoz Sabater et al., 2021)

[3] Slope based on ArcticDEM (Porter and et al., 2023).

[4] Soil bulk density at 100cm depth (Hengl and MacMillan, 2019)

The CR350 stations are additionally equipped with SnowVUE 10 ultrasonic snow-depth sensors Campbell Scientific, Inc. (2026b), which measure the temperature-compensated distance (TCDT) between the sensor and the underlying surface. The SnowVUE 10 uses a wide-band ultrasonic transducer to create sound pulses (50 kHz) that are reflected off the snow surface; by measuring the two-way travel time, distance is calculated using advanced spectrum analysis with accuracy of 0.2% of the distance to target and resolution of 0.1 mm. The measurement range extends from 0.4 to 10 m distance from the sensor, corresponding to snow depths of 0 to 9.6 m. The accuracy specification applies to still air with uniform temperature between the sensor and target; air movement, temperature gradients along the sonic path, snow density variations, and differences between actual and measured temperature can affect accuracy.

The CR350 stations employ Campbell Scientific 109 thermistor probes for soil temperature profiling. The 109 consists of a thermistor encapsulated in an epoxy-filled aluminum housing, with a measurement range of $-50$ to +70°C. Overall probe accuracy is a combination of thermistor interchangeability, bridge-resistor accuracy (0.1% tolerance, 10 ppm temperature coefficient), and Steinhart-Hart equation error Steinhart and Hart (1968). The manufacturer specifies total accuracy of approximately $\pm$0.4°C across the operating range, with interchangeability being the principal error component.

The HOBO H21-USB and U30 stations (e.g., Site 7 and 9) employ S-TMB-M002 12-bit temperature smart sensors Onset Computer Corporation (2026c) for both air and soil temperature measurements. These thermistor-based probes provide accuracy of $\pm$0.2°C within the 0 to 50°C range, with resolution of 0.03°C. At temperatures below 0°C, which characterize the

https://doi.org/10.5194/essd-2026-213
Preprint. Discussion started: 18 May 2026


Open Access Earth System Science Data Discussions

majority of the annual cycle in Arctic and subarctic Alaska, manufacturer specifications indicate degraded accuracy. Based on the manufacturer's accuracy curve, we conservatively estimate total uncertainty of ±0.4°C for measurements in the −20 to 0°C range and ±0.7°C for temperatures below −20°C. Long-term drift is specified as <0.1°C per year under normal operating conditions. For air temperature measurements, sensors are housed in RS3-B solar radiation shields to minimize radiative heating bias.

At each site, the approximate depth to the permafrost table is first determined using a manual steel frost probe (graduated metal rod). More specifically, the probe is inserted vertically into the ground until refusal at the frozen layer, providing an estimate of the active layer thickness at the time of installation. These measurements informed the selection of site-specific thermistor depths so that the sensor array captured both near-surface thermal conditions and temperature dynamics within the deeper portion of the active layer. Boreholes are then created using a narrow pointed metal probe to minimize disturbance to the surrounding soil structure. Prior to installation, thermistors were wired along a half-section PVC guide at the predetermined depths, forming a vertical sensor string. The guide is lowered into the borehole using two threaded halves of the PVC section to

**Table 5.** Summary of monitored variables, sensors, and dataloggers at each group of sites. Dataloggers are Campbell CR350 (CR350), Onset HOBO H21 (H21), and Onset HOBO U30 (U30).

| Variable | Sensor | Accuracy | Datalogger | | |
|---|---|---|---|---|---|
| | | | CR350 | H21 | U30 |
| Air temperature | ClimaVUE 40 / S-TMB-M002 | ±0.6°C[a] / ±0.2°C[b] | ✓ | ✓ | ✓ |
| Soil temperature (4 levels) | Campbell 109 / S-TMB-M002 | ±0.4°C[c] / ±0.2°C[b] | ✓ | ✓ | ✓ |
| Snow depth (TCDT) | SnowVUE 10 | 0.2% of distance[g] | ✓ | · | · |
| Solar flux density | ClimaVUE 40 | ±5% | ✓ | · | · |
| Precipitation (liquid) | ClimaVUE 40 | ±5% | ✓ | · | · |
| Lightning strike count | ClimaVUE 40 | >25% detection at <10 km | ✓ | · | · |
| Lightning strike distance | ClimaVUE 40 | Variable | ✓ | · | · |
| Wind speed | ClimaVUE 40 | 0.3 m/s or 3%[d] | ✓ | · | · |
| Vapor pressure | ClimaVUE 40 | ±0.2 kPa typical[e] | ✓ | · | · |
| Barometric pressure | ClimaVUE 40 | ±0.05 kPa at 25°C | ✓ | · | · |
| Relative humidity | ClimaVUE 40 | ±3% RH typical[f] | ✓ | · | · |

[a] ClimaVUE 40: ±0.6°C from −20 to 50°C after solar loading correction; ±0.2°C at 25°C. Non-aspirated sensor with firmware-based radiative correction.

[b] S-TMB-M002: ±0.2°C valid for 0 to 50°C only; accuracy degrades at sub-zero temperatures.

[c] Campbell 109: Combined accuracy from thermistor interchangeability, bridge resistor, and Steinhart-Hart equation.

[d] Whichever is greater.

[e] Varies with temperature and humidity.

[f] Unheated sensor; rime or frost may affect readings during cold, humid conditions.

[g] SnowVUE 10: Accuracy for still air with uniform temperature. Resolution 0.1 mm; range 0.4-10 m.

Site groupings by datalogger: CR350: Sites 3, 6; H21: Sites 7, 14; U30: Sites 4, 5, 9, 10, 11, 13, 15, 18.

https://doi.org/10.5194/essd-2026-213
Preprint. Discussion started: 18 May 2026




ensure proper positioning of the sensors along the soil column. Once the thermistor array reached the intended depth, the guide section is removed, leaving the sensors embedded directly within the native soil. We note that the upper probe (nominally 0 cm) records near-surface temperature beneath the moss or organic layer, while the deepest probe (typically 30-70 cm depending on site conditions) resolves longer-term thermal damping through the active layer.

## 3 Methods

### 3.1 Determination of Surface Freeze-Thaw Phenology

Surface FT phenology is derived from in situ ground temperature observations at the shallowest measurement depth (i.e., 0 cm) using a threshold-hysteresis method adapted from Chen et al. (2022). This approach captures the main seasonal phases of freezing and thawing without dependence on external satellite datasets, thereby ensuring site-specific consistency with subsurface thermal profiles. As can be seen in Fig. 4, daily soil temperature $T(t)$ at each site is classified into one of three instantaneous thermal states based on temperature thresholds $\theta_f = -0.1°\mathrm{C}$ and $\theta_t = +0.1°\mathrm{C}$:

$$\mathrm{State}(t) = \begin{cases} \text{Frozen}, & \text{if } T(t) \leq \theta_f \\ \text{Thawed}, & \text{if } T(t) \geq \theta_t \\ \text{Transitional}, & \text{if } \theta_f < T(t) < \theta_t \end{cases} \quad (1)$$

To prevent spurious short-term state changes caused by diurnal variability or measurement noise, a persistence of at least five consecutive days is considered for a valid transition, applied using a sliding window of 5 days and a minimum run length of the same duration. Each phase onset is defined as the first day satisfying the persistence criterion. We note that incomplete cycles at the beginning or end of the monitoring period are retained if their duration exceeds five days. We note that incomplete cycles at the beginning or end of the monitoring period are retained if their duration exceeds the five days duration.

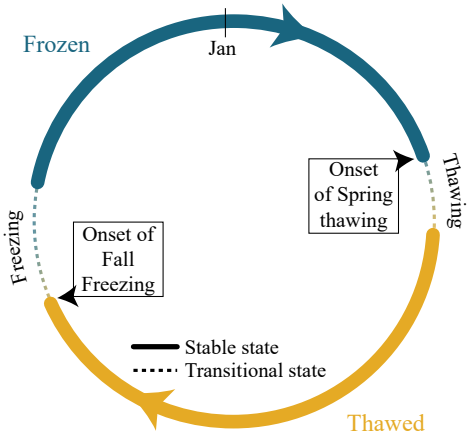


**Figure 4.** Simple diagram of the surface FT phenology and seasons.

https://doi.org/10.5194/essd-2026-213
Preprint. Discussion started: 18 May 2026




Following this classification, four primary FT phenology phases are identified:

- Thawing: Spring transition from frozen to thawed state
- Thawed: Stable thawed period during summer
- Freezing: Autumn transition from thawed to frozen state
- Frozen: Winter frozen state

This procedure provides seasonal windows whose timing and duration describe the phenological rhythm of the surface thermal regime independently of calendar year. The resulting FT chronology is used to compute depth-resolved averages of soil and air temperature as well as phase durations, enabling consistent comparison of seasonal soil thermal dynamics among the studied sites.

## 3.2 Derived variables

Multiple ground thermal and meteorological indicators are derived from the daily temperature records to characterize the subsurface thermal regime across the four surface FT phases and to enable inter-site comparison. The derived variables include the mean seasonal ground temperature (MSGT), thawing and freezing degree-days (TDD and FDD), and $n$-factors for thawed and frozen phases.

### 3.2.1 Mean Seasonal Ground Temperature

For each FT phase, the mean ground temperature is computed by averaging all daily soil temperatures within the corresponding seasonal window:

$$T_{g,s} = \frac{1}{N_s} \sum_{t=a_s}^{b_s} T_g(t), \tag{2}$$

where $a_s$ and $b_s$ represent the start and end dates of phase $s$, and $N_s$ is the number of valid daily observations in that phase.

### 3.2.2 Degree-day indices and $n$-factors

TDD and FDD are computed for both air and ground temperatures to quantify cumulative positive and negative thermal energy inputs within each FT phase (Klene et al., 2001; Karunaratne and Burn, 2003):

$$\mathrm{TDD} = \sum_{T_g>0} T_g, \qquad \mathrm{FDD} = \sum_{T_g<0} |T_g|, \tag{3}$$

where $T_g$ is the daily mean ground temperature. The corresponding indices for air temperature ($T_a$) are used to calculate the thawing and freezing $n$-factors:

$$n_t = \frac{\mathrm{TDD}_g}{\mathrm{TDD}_a}, \qquad n_f = \frac{\mathrm{FDD}_g}{\mathrm{FDD}_a}, \tag{4}$$

https://doi.org/10.5194/essd-2026-213
Preprint. Discussion started: 18 May 2026




where subscripts $g$ and $a$ denote ground and air, respectively. These factors express the degree of coupling between the atmosphere and the ground during the thawed and frozen periods, reflecting the effects of snow, vegetation, and soil moisture on heat transfer.

# 4 Results

## 4.1 Alaska-COLD Dataset Overview

Alaska-COLD is available online at: https://doi.org/10.5281/zenodo.17980271. Fig. 5 presents the mean diurnal temperature profiles at all sites, while Table 6 extends this picture by providing statistics over the complete monitoring period. The time series of the air and soil temperatures at each site, including ancillary meteorological and atmospheric for Sites 3 and 6, can be seen in Appendix Figs. A1 and A2 for reference. Interesting thermal structure aspects and variability between sites are revealed. In particular, the mean diurnal air temperature profiles span from -12.8°C to 0.2°C across all sites, with substantial variation in both absolute temperature and diurnal amplitude. The coldest site, (i.e., Site 15) farthest on the North Slope, maintains air temperatures between -12.8°C and -6.3°C throughout the day, while the warmest site, (i.e., Site 10) in the Brooks Foothills, ranges from -6.9°C to 0.2°C, briefly reaching above freezing during afternoon hours. Diurnal temperature ranges vary from $\approx$ 5°C at Sites 3 and 7 to 10°C at Site 10, reflecting differences in site characteristics. Nonetheless, all sites display the characteristic afternoon temperature maximum and early morning minimum typical of diurnal cycles.

In contrast to air, soil temperatures exhibit markedly dampened diurnal variability. Surface soil temperature amplitude is -6.8°C at Site 15 and 4.8°C at Site 14 across the daily cycle. Despite air temperature amplitudes of 3-7°C, surface soil diurnal amplitudes are substantially smaller, ranging from 0.7°C at Site 7 to 4.3°C at Site 4, with most sites exhibiting amplitudes below 2.5°C. The deepest sensors show virtually no diurnal structure, with temperature variations of only 0.004-0.047°C throughout the 24-hour period. This nearly isothermal behavior at depth demonstrates the strong attenuation of surface forcing through the soil column.

The vertical damping is accompanied by distinct thermal stratification patterns that vary among sites. At warmer interior locations (Site 4, 10, and 14), all soil depths remain above or near 0°C, with tightly clustered profiles indicating relatively uniform thermal conditions. The coldest North Slope sites maintain all soil layers well below freezing throughout the day, ranging from -2°C to -8°C. At these locations, the vertical spacing between different depth curves is compressed, reflecting uniform subfreezing conditions and limited vertical heat transfer. Intermediate sites show shallower soil temperatures oscillating around the freezing point while deeper layers remain consistently below 0°C, indicating active FT dynamics near the surface.

Over the complete monitoring period, the absolute air temperature extremes are severe: minimum air temperatures fall below -40°C at all sites, reaching -47.5°C at Site 14 in the Northern Brooks Foothills, while maximum air temperatures exceed 30°C at seven locations. Mean air temperatures span from -10.2°C at Site 7 to -3.4°C at Site 14. The mean daily hours below freezing ranges from 13.6 to 19.0 hours across sites, corresponding to 57-79% of day time spent at subfreezing temperatures.

Soil temperature extremes are substantially moderated relative to air. For instance, minimum surface soil temperatures range from -5.3°C at Site 7 to -19.7°C at Site 13, far warmer than the concurrent air temperature minima of -38°C to -48°C. This

https://doi.org/10.5194/essd-2026-213
Preprint. Discussion started: 18 May 2026


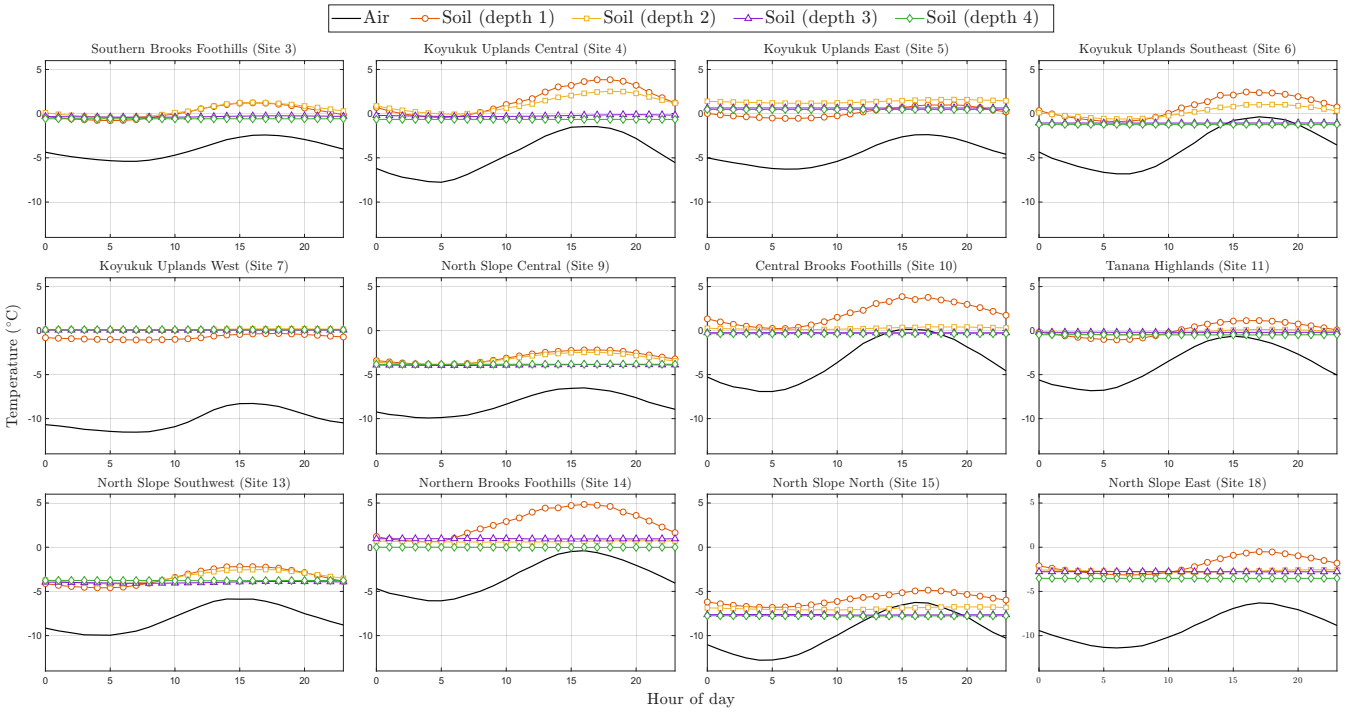


**Figure 5.** Mean diurnal temperature profiles of air and soil at four depths across all monitored sites (Depth 1 is the ground surface). Each curve represents the average hourly temperature over the entire observation period of its related site.

buffering reflects the insulating effect of snow cover and organic layers during winter. Maximum surface soil temperatures reach 16.7-39.9°C, with the highest values at Site 14. The annual range of monthly mean temperatures decreases systematically with depth: surface measurements show ranges of 11-26°C, intermediate depths exhibit 4-24°C, while the deepest sensors display only 2-12°C ranges. The median diurnal temperature amplitude likewise decreases from up to 1.5°C at the surface to less than 0.1°C at depth.

The progressive damping and filtering of temperature variability with depth is further quantified through Sample Entropy. Sample entropy is a metric that quantifies the randomness and predictability of a system (Pincus and Goldberger, 1994) (in this case temperature time series), with lower values indicating more regular temporal patterns. Air temperature entropy ranges from 0.18 to 0.50 across sites, consistently exceeding soil values. Soil entropy generally decreases with depth, from 0.02-0.17 at the surface to below 0.05 at the deepest measurements. This vertical gradient further reflects the progressive filtering of synoptic atmospheric variability through the soil column, with deeper layers exhibiting increasingly stable and predictable thermal regimes. Refer to Karevan and Suykens (2018) for more details about this measure.

https://doi.org/10.5194/essd-2026-213
Preprint. Discussion started: 18 May 2026


Open Access Earth System Science Data Discussions

**Table 6.** Summary statistics of the hourly air and soil temperature records at all monitored sites at the time of the publication of this manuscript. For each site and variable, values shown include mean temperature (°C), mean daily hours below freezing ($\leq 0$°C), median diurnal range (°C), the number of FT transitions, and Sample Entropy ($m = 2$, $r = 0.2\times$SD, Chebyshev distance) over the full observation period. Soil rows report [min, max] ranges across the four soil layers.

| ID | Site | Temp. | Height /Depth | Mean | Freeze Frac. | Diurnal Range | FT Count | Sample Entropy |
|---|---|---|---|---|---|---|---|---|
| 3 | Southern Brooks Foothills | Air | 1.5m | -4.01 | 14.53 | 5.02 | 134 | 0.37 |
| | | Soil | [0-45.1cm] | [-0.58,0.36] | [15.31,17.31] | [0.03,1.45] | [8,60] | [0.04,0.17] |
| 4 | Koyukuk Uplands Central | Air | 1.5m | -4.61 | 14.30 | 8.62 | 246 | 0.24 |
| | | Soil | [0-40.9cm] | [-0.65,1.52] | [14.60,18.99] | [0.03,0.44] | [26,72] | [0.01,0.04] |
| 5 | Koyukuk Uplands East | Air | 1.5m | -4.49 | 14.32 | 5.99 | 132 | 0.29 |
| | | Soil | [0-59.8cm] | [0.17,1.37] | [12.23,15.50] | [0.03,0.24] | [28,150] | [0.02,0.07] |
| 6 | Koyukuk Uplands Southeast | Air | 1.5m | -3.69 | 13.57 | 8.15 | 218 | 0.50 |
| | | Soil | [0-48.3cm] | [-1.21,0.71] | [14.14,19.30] | [0.01,0.90] | [12,42] | [0.01,0.20] |
| 7 | Koyukuk Uplands West | Air | 1.5m | -10.15 | 18.90 | 5.54 | 66 | 0.18 |
| | | Soil | [0-49.4cm] | [-0.74,0.13] | [4.79,20.03] | [0.03,0.14] | [1,15] | [0.02,0.09] |
| 9 | North Slope Central | Air | 1.5m | -8.33 | 16.72 | 6.55 | 138 | 0.18 |
| | | Soil | [0-34cm] | [-3.91,-3.04] | [16.33,17.39] | [0.14,0.79] | [59,118] | [0.01,0.06] |
| 10 | Central Brooks Foothills | Air | 1.5m | -3.47 | 13.61 | 10.00 | 130 | 0.27 |
| | | Soil | [0-69.8cm] | [-0.34,1.91] | [14.99,16.97] | [0.03,0.29] | [10,48] | [0.02,0.04] |
| 11 | Tanana Highlands | Air | 1.5m | -3.82 | 13.94 | 9.43 | 270 | 0.29 |
| | | Soil | [0-55.3cm] | [-0.48,0.07] | [11.29,15.53] | [0.06,0.97] | [12,129] | [0.02,0.07] |
| 13 | North Slope Southwest | Air | 1.5m | -8.02 | 16.66 | 7.56 | 162 | 0.21 |
| | | Soil | [0-31.5cm] | [-3.98,-3.35] | [16.45,17.32] | [0.12,1.05] | [24,82] | [0.01,0.06] |
| 14 | Northern Brooks Foothills | Air | 1.5m | -3.37 | 13.73 | 8.85 | 94 | 0.23 |
| | | Soil | [0-72cm] | [-0.01,2.68] | [9.56,17.03] | [0.06,0.83] | [2,60] | [0.01,0.07] |
| 15 | North Slope North | Air | 1.5m | -9.64 | 17.41 | 9.99 | 35 | 0.39 |
| | | Soil | [0-34.5cm] | [-7.76,-5.92] | [18.83,23.46] | [0.10,0.31] | [1,3] | [0.01,0.04] |
| 18 | North Slope East | Air | 1.5m | -9.02 | 16.29 | 8.82 | 72 | 0.22 |
| | | Soil | [0-37cm] | [-3.52,-1.99] | [14.40,17.77] | [0.11,0.54] | [2,36] | [0.01,0.03] |

### 4.2 Data Evaluation

The FT phenology analysis reveals distinct spatial patterns across north-central Alaska (see Fig. 6). The four FT phases exhibit markedly different timescales: thawed and frozen conditions represent the longest observed phases, whereas transitional thaw-

https://doi.org/10.5194/essd-2026-213
Preprint. Discussion started: 18 May 2026


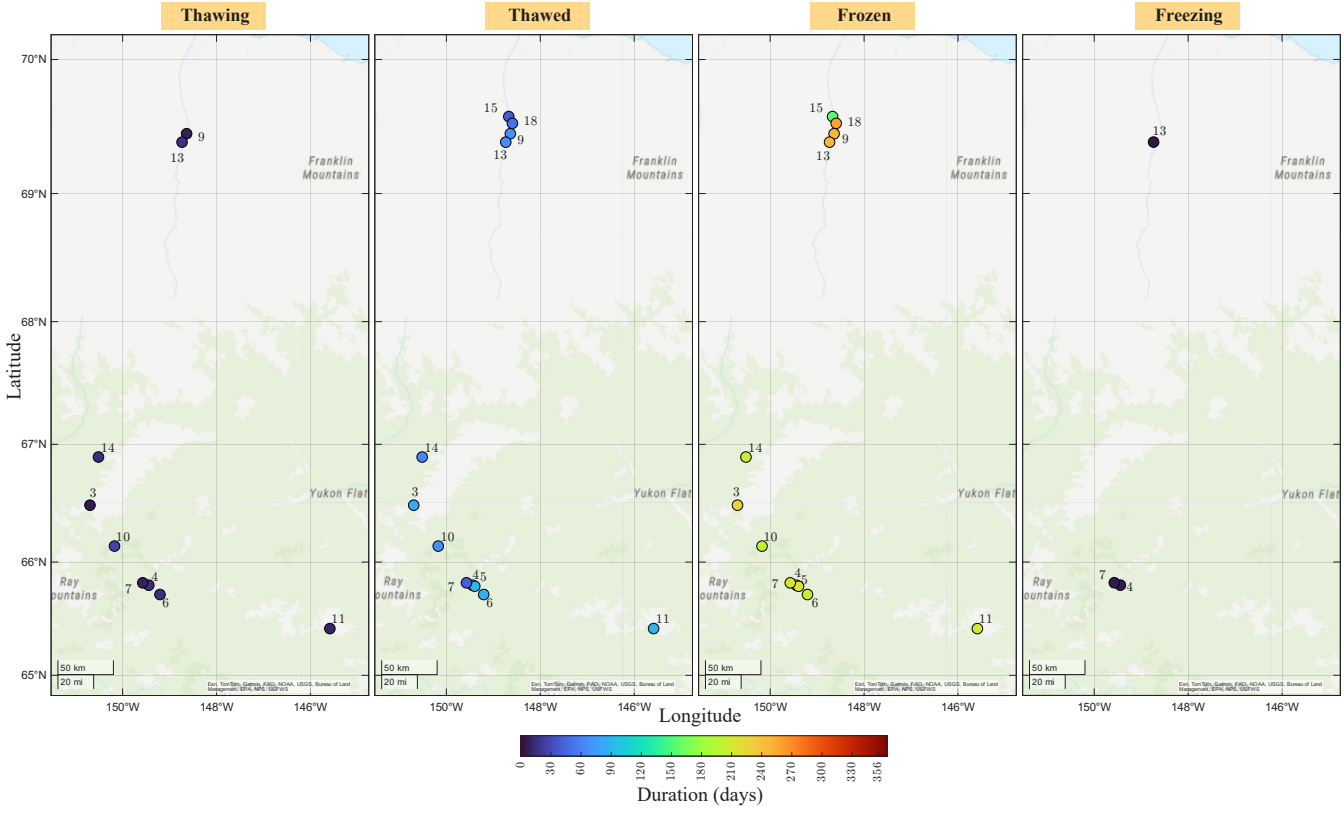


**Figure 6.** Spatial patterns of the average duration of FT phenology phases across monitored sites in north-central Alaska. Values represent phase-specific averages over available years at each site.

ing and freezing periods are comparatively brief. Across sites, thawed durations range from 39 days at Site 15 to 89.7 days at Site 5, while frozen durations range from 155 days at Site 15 to 254 days at Site 18.

The thawed phase shows a clear north-south contrast, although with site-specific variability. Northern sites, including Sites 9, 13, 15, and 18, show shorter thawed periods of approximately 39-69.7 days. In contrast, several interior sites exhibit longer thawed periods, particularly Sites 4, 5, 6, and 11, where thawed durations reach approximately 86.3-89.7 days. Site 3 also shows a relatively long thawed duration of 82.7 days, whereas Sites 7, 10, and 14 show shorter to intermediate thawed durations of 40-66.5 days.

The frozen phase generally exhibits the opposite spatial tendency, with longer frozen durations at the northern sites. Sites 9, 13, and 18 remain frozen for approximately 244-254 days, corresponding to about 67-70% of a year. However, Site 15 is an exception, with a frozen duration of 155 days and no recorded transitional duration in the table, suggesting that this value should be interpreted cautiously. Interior sites generally show shorter frozen durations, mostly between 197 and 224 days. Where both transitional phases are available, thawing tends to last longer than freezing. Thawing durations range from 5 to 27

https://doi.org/10.5194/essd-2026-213
Preprint. Discussion started: 18 May 2026


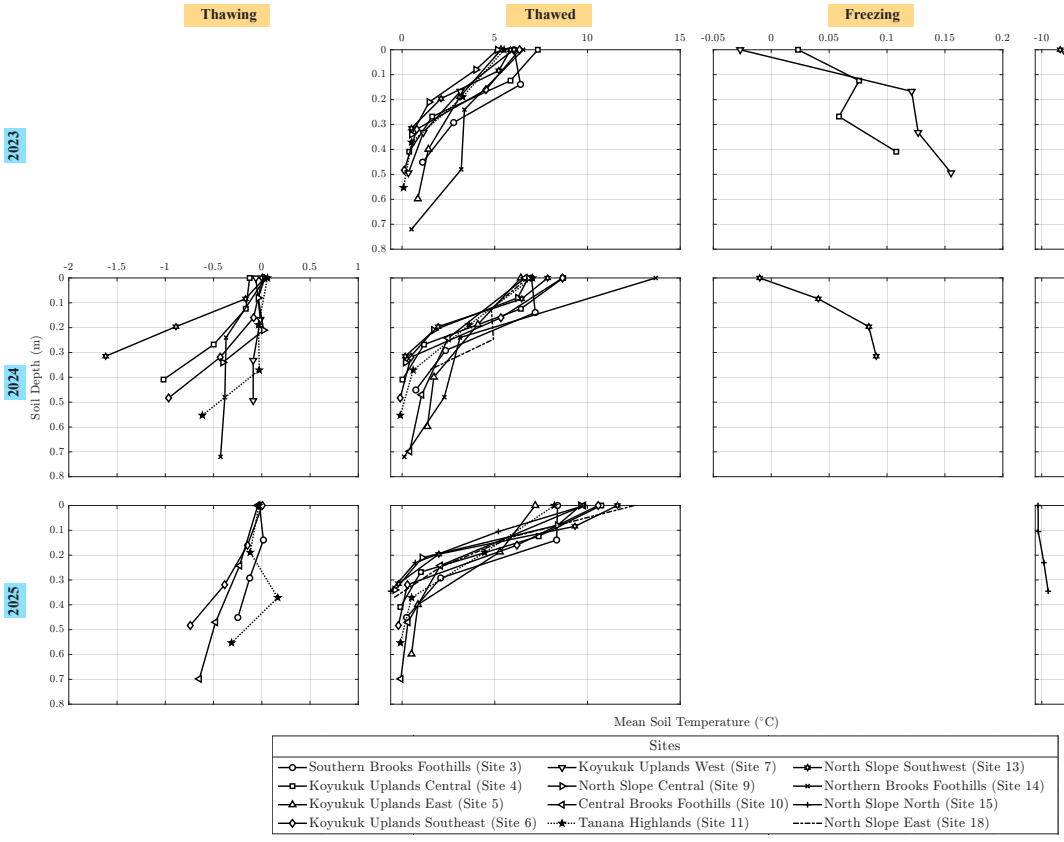


**Figure 7.** Mean ground temperature profiles across depths for all sites, grouped by surface FT phenology phases and by year. Daily soil temperatures were averaged by depth within each FT phase and aggregated by year. The profiles show seasonal thermal stratification, depth-dependent thermal damping, and near-zero transitional behavior associated with FT phase changes

days, whereas freezing durations range only from 4 to 5 days. However, freezing durations are available for only three sites, so this asymmetry should be interpreted cautiously.

Vertical temperature stratification within the soil column exhibits pronounced seasonal reversals across FT phenology phases (see Fig. 7). During thawed periods, mean soil temperatures are highest near the surface and decrease with depth. Surface values at 0 m range from approximately 5.1 to 13.7°C, while temperatures at 0.45-0.72 m remain much closer to the freezing point, ranging from about -0.2 to 3.2°C. During frozen periods, the thermal gradient reverses: surface temperatures decrease to approximately -10.2 to -2.1°C, whereas deeper sensors at 0.45-0.72 m remain comparatively buffered, ranging from about -2.1 to 0.2°C. These patterns indicate strong seasonal thermal damping with depth and substantial site-to-site variability in the penetration of winter cooling through the measured soil column.

The transitional thawing and freezing phases are characterized by near-zero soil temperatures, consistent with phase-change buffering during FT transitions. During the thawing phase, available profiles from 2024-2025 remain close to 0°C near the

https://doi.org/10.5194/essd-2026-213
Preprint. Discussion started: 18 May 2026


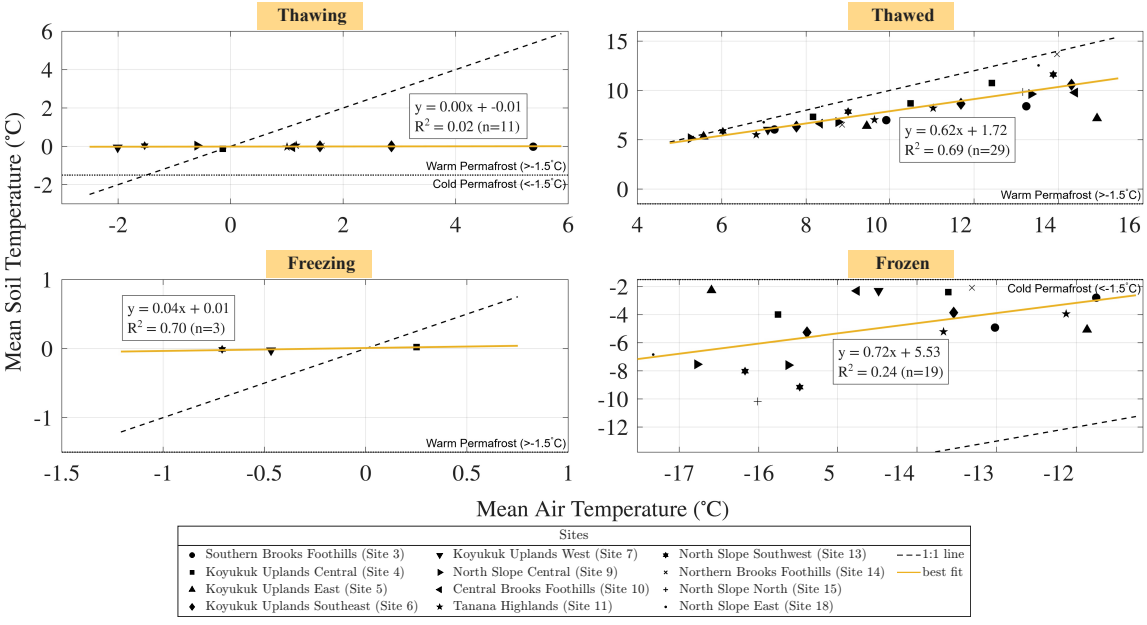


**Figure 8.** Relationship between mean air temperatures and mean ground surface temperature across FT phenology phases. Each point represents a site-year average during one FT phase, and regression lines are fitted separately for each phase.

surface but become weakly subzero at depth, with values ranging overall from approximately -1.6 to 0.2°C. During the freezing phase, available profiles from 2023-2024 show tighter clustering around 0°C, with temperatures ranging from approximately -0.03 to 0.16°C across the measured profile. Although the limited number of freezing phase profiles should be considered when interpreting interannual patterns, this near-isothermal behavior seems to be consistent with latent-heat effects during freezing and thawing.

These vertical thermal patterns are accompanied by systematic variations in air-ground coupling across the annual FT cycle (see Fig. 8). During the thawing phase, mean ground surface temperatures remain tightly clustered near 0°C despite mean air temperatures ranging from approximately -2.0 to 5.4°C. The fitted relation is nearly flat (slope = 0.003, $R^2$ = 0.02, n = 11), indicating strong thermal buffering during the thawing transition.

In the thawed phase, air-ground coupling strengthens substantially (slope = 0.62, $R^2$ = 0.69, n = 29). Mean ground surface temperatures range from approximately 5.1 to 13.7°C, while mean air temperatures range from 5.3 to 14.9°C. The regression line remains below the 1:1 reference, indicating that ground surface temperatures are generally cooler than air temperatures during thawed conditions, but still respond strongly to air-temperature variability.

The freezing phase shows near-zero ground surface temperatures, with MAGT ranging only from approximately -0.03 to 0.02°C while MAAT ranges from -0.71 to 0.25°C. Although the fitted $R^2$ is high (0.70), this relationship is based on only three site-year observations and has a near-zero slope (0.04). Therefore, the freezing-phase pattern seems to be evidence of a phase-change buffering near 0°C rather than a robust air-ground coupling.

https://doi.org/10.5194/essd-2026-213
Preprint. Discussion started: 18 May 2026


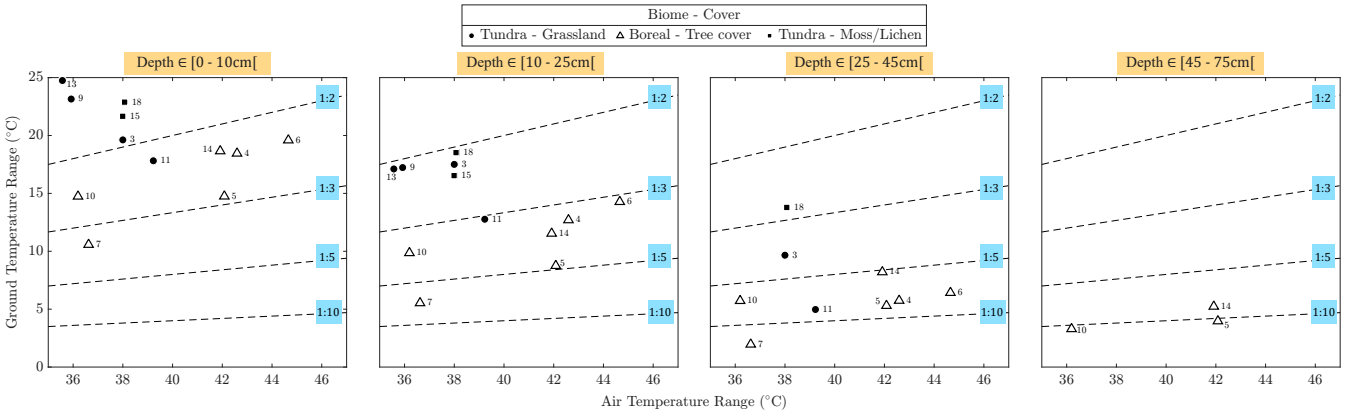


**Figure 9.** Relationship between annual air and ground temperature ranges across standardized depth bins for all study sites. Daily temperatures were aggregated to monthly means, and soil profiles were linearly interpolated to common depth intervals to enable cross-site comparison despite differing probe depths. The panels illustrate progressive damping of ground temperature variability with depth and differences in coupling strength between tundra and boreal surfaces.

Under fully frozen conditions, mean ground surface temperatures are consistently warmer than mean air temperatures. MAGT ranges from approximately -10.2 to -2.1°C, whereas MAAT ranges from -17.3 to -11.8°C, producing a positive winter thermal offset of approximately 5.8 to 14.3°C. The frozen-phase regression shows a moderate slope but weak explanatory power (slope = 0.72, $R^2$ = 0.24, n = 19), suggesting that winter ground temperatures might be influenced not only by air temperature but also by site-specific surface and subsurface controls. Several Koyukuk and Brooks Foothills sites plot near the warmer end of the frozen-ground range, whereas North Slope sites generally show colder ground surface temperatures.

Overall, the divergence from the 1:1 reference line indicates that air temperature alone does not determine ground surface temperature across the FT cycle. Instead, the phase-dependent patterns are consistent with stronger atmospheric coupling during thawed conditions, latent-heat buffering during transitional phases, and winter insulation or surface-offset effects during frozen conditions.

At the annual scale, these phase-dependent coupling patterns integrate into systematic damping of temperature variability with depth. Indeed, progressive attenuation of atmospheric temperature is clearly seen in Fig. 9. Near-surface measurements (0-10 cm) exhibit ground temperature ranges of 11-25°C, representing roughly one-quarter to two-thirds of air temperature ranges (36-45°C). At intermediate depths (10-45 cm), temperature ranges decrease progressively: the 10-25 cm interval shows 6-19°C, while the 25-45 cm interval drops to 2-14°C. By 45-75 cm depth, ground temperature ranges decline dramatically to only 3-5°C despite air ranges of 36-42°C, approaching the nearly constant temperatures characteristic of the permafrost body below the depth of zero annual amplitude. At the deepest interval (45-75 cm), systematic damping patterns emerge. The three sites with measurements at this depth all exhibit boreal tree cover and achieve strong damping ratios of 1:8 to 1:11, maintaining ground temperature ranges of 3-5°C for air ranges of 36-42°C.

https://doi.org/10.5194/essd-2026-213
Preprint. Discussion started: 18 May 2026


Open Access Earth System Science Data Discussions

**Table 7.** Average values of derived parameters at the study sites.

| ID | Sites (n cycles) | $n_{Thawed}$ | TDD | $n_{Frozen}$ | FDD |
|---|---|---|---|---|---|
| 3 | Southern Brooks Foothills (3) | 0.7075 | 417.07 | 0.3061 | 866.65 |
| 4 | Koyukuk Uplands Central (3) | 0.9264 | 601.44 | 0.2136 | 672.26 |
| 5 | Koyukuk Uplands East (3) | 0.5740 | 349.7 | 0.2738 | 824.36 |
| 6 | Koyukuk Uplands Southeast (3) | 0.7768 | 567.18 | 0.3116 | 933.38 |
| 7 | Koyukuk Uplands West (1) | 0.8474 | 246.43 | 0.1572 | 489.9 |
| 9 | North Slope Central (3) | 0.8265 | 342.8 | 0.4663 | 1858 |
| 10 | Central Brooks Foothills (2) | 0.7290 | 452.7 | 0.1561 | 456.96 |
| 11 | Tanana Highlands (3) | 0.7802 | 480.42 | 0.3512 | 948.86 |
| 13 | North Slope Southwest (3) | 0.8774 | 350.93 | 0.5422 | 2098.6 |
| 14 | Northern Brooks Foothills (2) | 1.0192 | 653.94 | 0.1543 | 433.63 |
| 15 | North Slope North (1) | 0.7919 | 235.5 | - | - |
| 18 | North Slope East (2) | 0.9548 | 328.18 | 0.3921 | 1743.7 |

In terms of biomes, systematic differences in damping efficiency emerge across all depth intervals. Boreal tree-covered sites (e.g., Site 5) consistently exhibit stronger damping than tundra sites (e.g., Site 3), with the separation intensifying with depth. At the surface (0-10 cm), boreal sites show mean damping ratios of 1:2.6 compared to 1:1.8 for tundra sites. By 10-25 cm depth, this difference amplifies: boreal sites achieve 1:3.1-6.6 while tundra sites show 1:2.1-3.1. At the deepest measured interval (45-75 cm), three boreal sites maintain damping ratios of 1:8.0-11.0, with ground temperature ranges of only 3-5°C despite air ranges of 36-42°C.

Within the tundra biome, distinct sub-patterns emerge. Grassland tundra sites (e.g., Site 3) exhibit moderate damping (1:1.4-2.2 at surface) with high ground temperature variability (18-25°C). Moss/lichen tundra sites (i.e., Sites 15 and 18) display the weakest damping in the network (1:1.7-2.8), maintaining ground temperature ranges of 14°C even at 25-45 cm depth.

The cumulative effect of these thermal regimes is quantified through degree-day metrics, as reported in Table 7. TDD range from 236°C·days at Site 15 on the North Slope to 654°C·days at Site 14 in the Brooks Foothills, tracking both the duration of the thaw season and the intensity of summer warmth. The interior and transitional sites (Sites 4, 6, and 14) accumulate 567-654°C·days, sufficient to drive active layer depths of 50-100 cm depending on soil properties and moisture content. In contrast, northern coastal sites accumulate only 236-351°C·days, limiting active layer development to 30-60 cm and reflecting the maritime-influenced summer conditions of the Arctic coastal plain.

On the other hand, FDD displays even starker contrasts, ranging from 434°C·days at Site 14 near the Brooks Range to 2099°C·days at Site 13 on the North Slope. The Deadhorse cluster (i.e., Sites 9, 13, and 18) consistently records the highest FDD (1744-2099°C·days), reflecting prolonged extreme cold, and probable persistent katabatic winds from the Brooks Range and minimal snow insulation. Interior sites (i.e., Sites 10, 4, and 14) accumulate only 434-672°C·days despite experiencing

https://doi.org/10.5194/essd-2026-213
Preprint. Discussion started: 18 May 2026




similar or colder minimum air temperatures, most likely demonstrating the influence of winter insulation in determining the ground thermal regime.

The FDD/TDD ratio provides a useful index of relative seasonal forcing. Ratios above 5:1 (North Slope Sites 9, 13, and 18: 5.3-6.0) indicate strongly cold-dominated thermal regimes characteristic of continuous permafrost with mean annual ground temperatures well below -5°C at depth. Site 10 near the Brooks Range shows a nearly balanced ratio (1.01), while the nearby Site 14 exhibits a remarkable thaw-dominated regime (0.66), with TDD exceeding FDD. This exceptionally low FDD/TDD ratio suggests highly vulnerable "warm permafrost" conditions where modest shifts in thermal regimes could move the system toward seasonal freezing or complete permafrost loss.

### 4.3 Comparison with ERA5-Land

To provide an external consistency check for Alaska-COLD, hourly station observations are compared with co-located ERA5-Land temperature estimates (see Table A1). Near-surface air temperature showed strong agreement with ERA5-Land temperature_2m across the 12 monitoring sites, with $R^2$ values ranging from 83% to 92%, RMSE values of 3.7-6 °C, and biases between -2 and 1.8 °C. This agreement indicates that the Alaska-COLD air-temperature records capture temporal atmospheric variability that is broadly consistent with the established gridded reanalysis product.

However, agreement is weaker and less consistent for soil temperature. The comparison between observed near-surface soil temperature and ERA5-Land skin_temperature showed consistently negative $R^2$ values, relatively large errors, and cold biases at all sites. In contrast, comparisons with ERA5-Land soil_temperature_level_1-3 showed mixed behavior: some shallow subsurface comparisons produced moderate agreement, but many deeper-layer comparisons had negative $R^2$ values and positive biases. These patterns are expected as ERA5-Land provides grid-cell-scale modeled layer temperatures while Alaska-COLD provides point-scale in situ measurements influenced by local surface, snow, soil, vegetation, and hydrological conditions.

These results are consistent with previous evaluations of ERA5-Land and other reanalysis soil-temperature products in high-latitude environments. For instance, Cao et al. Cao et al. (2020) reported warm ERA5-Land soil-temperature biases in northern Canada and Alaska, partly linked to model structure, snow representation, and soil-column discretization. In a follow up article, Cao et al. Cao et al. (2022) further showed that improving snow-layer representation can reduce winter soil-temperature warm biases in high-latitude permafrost regions. More broadly, Herrington et al. Herrington et al. (2024) found that Arctic reanalysis soil temperatures can have substantial RMSE and seasonally varying skill relative to in situ observations.

## 5 Discussion

### 5.1 Data Acquisition and Quality Assurance

The Alaska-COLD network spans remote locations across north-central Alaska, necessitating extensive field campaigns via the Dalton and Steese Highways with logistical support from Yukon River, Coldfoot, and Deadhorse camps. Seasonal site visits involved downloading data, replacing batteries, and collecting complementary measurements including snow depth and density

https://doi.org/10.5194/essd-2026-213
Preprint. Discussion started: 18 May 2026


using standard field equipment (shovel, tape measure, 1-liter metal wedge, scale). Repairs were performed opportunistically during these visits.

Two significant equipment failures occurred during the monitoring period. Site 15 experienced complete datalogger failure in 2024, recording only a single data point after initialization. The unit was replaced during the 2025 field campaign, resulting in a substantial data gap. Site 14 site suffered battery depletion that halted logging; the system recovered after solar panel cleaning and battery recharging. These failures highlight the challenges of autonomous remote monitoring in harsh Arctic conditions, where extreme cold (-40°C air temperatures), persistent wind, and limited solar radiation during winter months stress power systems and electronics. Future deployments should consider redundant power systems and datalogger backup units at the most remote sites.

Data quality is maintained through pre-deployment ice-bath calibration of all temperature sensors (accuracy ±0.2°C for soil probes, ±0.6°C for air temperature), hourly logging intervals to capture diurnal dynamics, and post-processing quality checks for sensor drift, outliers, and discontinuities. Despite these precautions, the dataset has variable temporal coverage, with seven sites providing 714-726 days of continuous records (2-3 complete FT cycles) while others have gaps or shorter monitoring periods. Researchers using the dataset should consider the monitored duration when selecting sites for specific analyses.

### 5.2 Thermal Regime Heterogeneity and Permafrost Vulnerability

The dataset documents substantial spatial variability in permafrost thermal regimes across modest geographic scales, with FDD/TDD ratios spanning from 0.66 (i.e., thaw-dominated) to 6.0 (i.e., strongly cold-dominated) within approximately 300 km. This heterogeneity challenges single-parameter predictions of permafrost distribution based solely on mean annual air temperature (Zhang et al., 2005). The pronounced winter thermal offset (8-14°C ground-air temperature difference at interior sites) demonstrates that MAGT can substantially exceed MAAT where winter insulation is strong, creating "protected but vulnerable" permafrost; sites maintaining temperatures near 0°C at depth despite cold atmospheric conditions.

Site 14 in the Brooks Foothills exemplifies extreme vulnerability, with FDD/TDD = 0.66. This thaw-dominated regime suggests the site exists near a critical threshold where modest thermal shifts, earlier snowmelt, or vegetation disturbance could trigger permafrost loss. Given projected thermal shifts in Alaska of 1.5-5.0°C (Manos et al., 2025), sites with strong thermal insulation and near-threshold ground temperatures face disproportionate risk despite currently experiencing cold air temperatures. Alaska-COLD provides baseline observations essential for detecting future changes in these transitional permafrost zones.

### 5.3 Vegetation Control on Thermal Damping

Systematic differences in thermal damping between boreal (1:2.6 at surface, 1:8-11 at depth) and tundra sites (1:1.8 at surface) demonstrate vegetation as a common discriminator of ground thermal regimes. Boreal forests achieve efficient damping through combined canopy shading, snow trapping, and thick organic soil horizons (Stuenzi et al., 2021), maintaining ground temperatures 2-5°C cooler in summer and up to 10°C warmer in winter than tundra sites. This multi-scale thermal regulation is critical for permafrost persistence under shifting environmental conditions (Zhao et al., 2025).

https://doi.org/10.5194/essd-2026-213
Preprint. Discussion started: 18 May 2026


However, the weakest damping observed at moss/lichen tundra sites (1:1.7-2.8) contradicts expectations given cryptogams' reputation as thermal insulators (Blok et al., 2011; Porada et al., 2016). This can be attributed to site-specific factors: wind-exposed coastal positions limiting snow accumulation, high moisture content increasing thermal conductivity, and potentially thin cryptogamic layers. This finding underscores that vegetation type alone is insufficient for predicting thermal regimes; other aspects such as exposure, snow regime, and organic horizon depth might be needed. Current land surface models often parameterize thermal properties by broad vegetation classes (Biskaborn et al., 2019); the Alaska-COLD dataset provides ground-truth for developing more nuanced, process-based representations of surface-atmosphere thermal coupling across heterogeneous Arctic landscapes.

## 6 Conclusions

The Alaska-COLD dataset comprises high-temporal-resolution in situ observations from multiple sites across Alaska's permafrost regions. The sites cover boreal forest, interior upland, Brooks Foothills, and Arctic tundra settings. The dataset currently holds hourly near-surface air temperature and soil temperature measurements at multiple depths down to 0.7 m from 12 monitoring sites.

From these hourly records, FT phenology is classified into thawing, thawed, freezing, and frozen phases. In addition, several variables were derived to characterize surface energy exchange and subsurface thermal behavior, including $n$-factors, degree-day, and damping-related metrics. Key findings include: (1) strong depth-dependent thermal damping, with surface-soil diurnal amplitudes of 0.7-4.3°C decreasing to only 0.004-0.047°C at the deepest sensors, and annual ground-temperature ranges declining from 11-25°C near the surface to 3-5°C at 45-75 cm depth; (2) phase-dependent air-ground coupling, characterized by strong thermal buffering near 0°C during transitional phases, the strongest coupling during thawed conditions, and positive winter thermal offsets of approximately 6-14°C during frozen conditions; and (3) spatial variability in FT phenology, with longer thawed periods at several interior sites and longer frozen periods at most northern sites. In addition, the comparison with co-located ERA5-Land hourly estimates further showed stronger agreement for air temperature than for soil temperature. This highlights both the external consistency of the air-temperature records and the added value of Alaska-COLD for resolving site-level soil thermal dynamics.

Dataset limitations include variable temporal coverage (44-726 days), equipment failures causing gaps at two sites, and absence of co-located snow depth and radiation measurements. Despite these constraints, the systematic monitoring of thermal regimes enables applications in remote sensing validation, machine learning development, and environmental modeling. Continued data collection and planned enhancements (snow measurements, additional meteorological variables, satellite data integration) will strengthen the network's value for understanding permafrost response atmospheric conditions.

https://doi.org/10.5194/essd-2026-213
Preprint. Discussion started: 18 May 2026




## 7 Data availability

The Alaska-COLD dataset used in this study is openly available under a Creative Commons Attribution 4.0 International (CC BY 4.0) license on Zenodo (Ahajjam, 2025). The dataset can be accessed at https://doi.org/10.5281/zenodo.17980272. A mirrored copy is also hosted within the Defense Resiliency Platform Against Extreme Cold Weather at https://drp.dataone.org/urn:uuid:67c4acb4-5ad7-43c0-98ea-da70cb17654e.

*Author contributions.* A. Ahajjam: Conceptualization, Methodology, Investigation, Data curation, Writing – original draft, Writing – review & editing, and Visualization. A. Caparó Bellido: Conceptualization, Methodology, Investigation, Visualization, Data curation, Writing – original draft, and Writing – review & editing. A. Wilcox: Methodology, Investigation, Writing – original draft, and Writing – review & editing. M. Soaper: Data curation, Investigation and Validation, Writing – review & editing. H. Patterson: Data curation, Investigation and Validation, Writing – review & editing. S. Weaver: Investigation and Validation, Writing – review & editing. S. Kidanu: Supervision, Investigation and Validation, Writing – review & editing. T. Pasch: Funding acquisition, Supervision, Writing – review & editing, Conceptualization, and Resources.

*Competing interests.* The authors declare that they have no conflict of interest.

*Acknowledgements.* The authors thank Jaakko Putkonen for his assistance with field data acquisition in Alaska.

DISTRIBUTION A: Approved for Public Release. Distribution is Unlimited. This material is based upon work supported by the Broad Agency Announcement Program and the Cold Regions Research and Engineering Laboratory (ERDC-CRREL) under Contract No. W913E524C0017.

https://doi.org/10.5194/essd-2026-213
Preprint. Discussion started: 18 May 2026


Open Access Earth System Science Data Discussions

## Appendix A

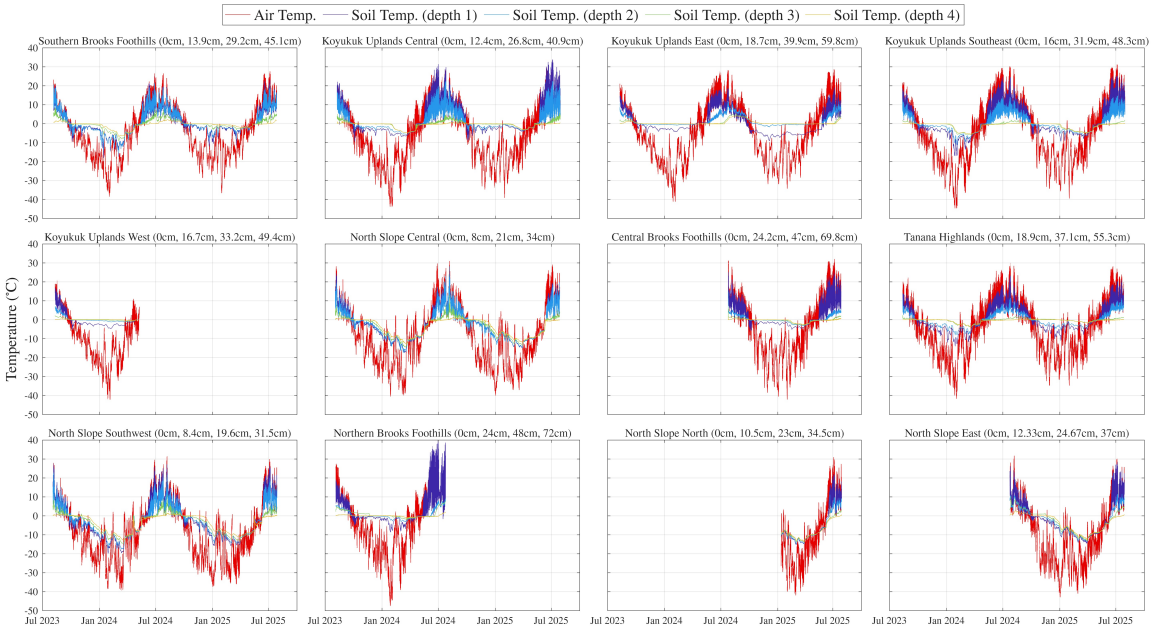


**Figure A1.** Time series of air and soil temperatures recorded at all sites from July 2023 to July 2025.

https://doi.org/10.5194/essd-2026-213
Preprint. Discussion started: 18 May 2026


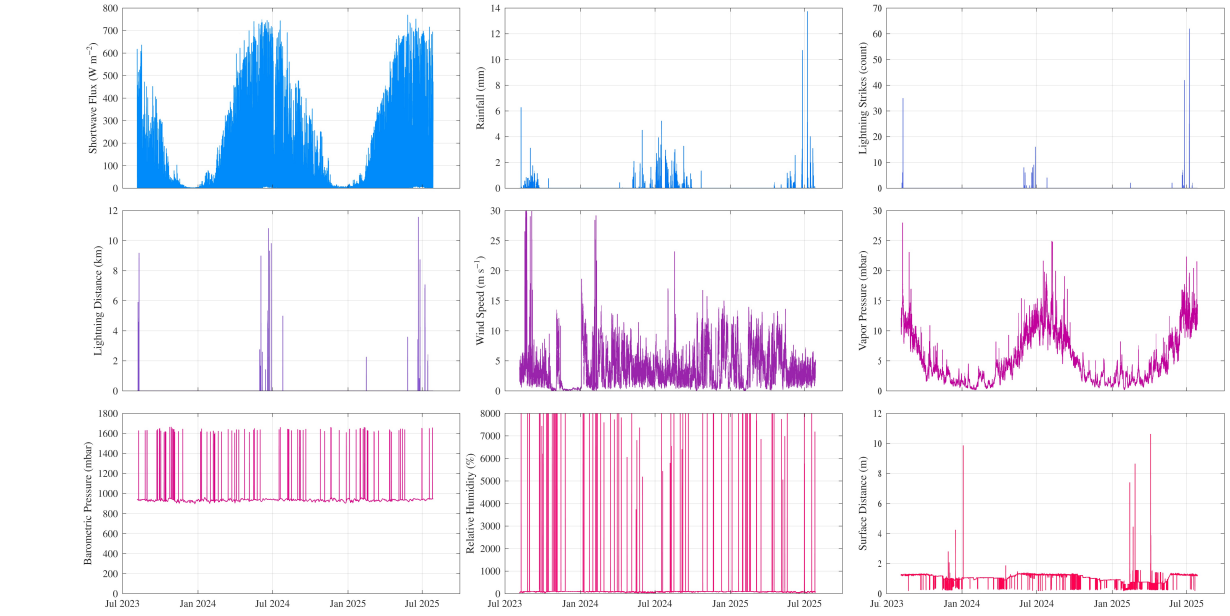


(a) Southern Brooks Foothills

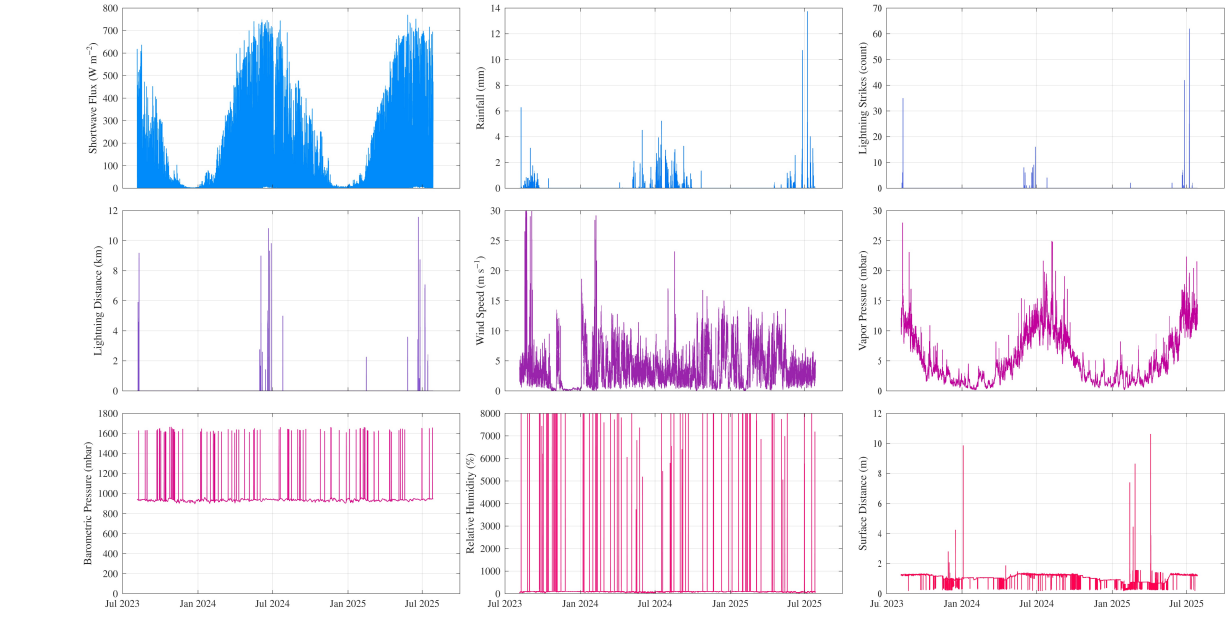


(b) Koyukuk Uplands Southeast

**Figure A2.** Time series of ancillary meteorological and atmospheric variables recorded at the Southern Brooks Foothills and Koyukuk Uplands Southeast sites (id: 3 and 6) from July 2023 to July 2025.

https://doi.org/10.5194/essd-2026-213
Preprint. Discussion started: 18 May 2026


Open Access Earth System Science Data Discussions

**Table A1.** Comparison summary between Alaska-COLD and ERA5-Land. Metrics are computed from hourly co-located records. Air temperature is compared with ERA5-Land's temperature_2m, while Soil temperatures are compared against skin_temperature and soil_temperature_level_1-3, respectively. Soil rows report [min, max] ranges across the four soil layers. n is the number of matched samples. Bias is computed as the difference between ERA5-Land and Alaska-COLD temperatures, with positive values indicate warmer ERA5-Land temperature estimates.

| ID | Site name | Temp. | n | $R^2$ | Bias (°C) | RMSE (°C) | MAE (°C) |
|---|---|---|---|---|---|---|---|
| 3 | Southern Brooks Foothills | Air | 17322 | 0.921 | -0.100 | 3.699 | 2.873 |
| | | Soil | 17322 | [-5.422, 0.640] | [-5.589, 2.659] | [3.760, 12.257] | [2.585, 9.078] |
| 4 | Koyukuk Uplands Central | Air | 17320 | 0.865 | 0.865 | 5.502 | 4.235 |
| | | Soil | 17320 | [-14.843, 0.442] | [-6.016, 3.278] | [3.914, 13.469] | [2.401, 10.096] |
| 5 | Koyukuk Uplands East | Air | 17227 | 0.908 | 0.635 | 4.398 | 3.567 |
| | | Soil | 17227 | [-20.765, -1.944] | [-4.779, 2.116] | [4.534, 13.130] | [2.772, 9.788] |
| 6 | Koyukuk Uplands Southeast | Air | 17050 | 0.896 | 0.249 | 4.943 | 3.903 |
| | | Soil | 17050 | [-11.042, -0.070] | [-4.869, 4.517] | [5.113, 12.381] | [3.566, 9.511] |
| 7 | Koyukuk Uplands West | Air | 6539 | 0.880 | 0.278 | 4.286 | 3.357 |
| | | Soil | 6539 | [-457.226, -3.529] | [-10.413, 1.450] | [3.397, 16.414] | [2.566, 12.434] |
| 9 | North Slope Central | Air | 17420 | 0.868 | 0.156 | 5.365 | 4.128 |
| | | Soil | 17420 | [-1.531, 0.443] | [-5.682, 4.508] | [5.234, 12.751] | [4.349, 9.941] |
| 10 | Central Brooks Foothills | Air | 8828 | 0.857 | 0.329 | 5.746 | 4.485 |
| | | Soil | 8828 | [-41.608, -3.143] | [-5.674, 3.426] | [5.313, 12.374] | [3.419, 9.394] |
| 11 | Tanana Highlands | Air | 17135 | 0.830 | -1.563 | 5.629 | 4.466 |
| | | Soil | 17135 | [-27.347, -0.216] | [-7.488, 1.943] | [4.134, 13.245] | [2.656, 10.229] |
| 13 | North Slope Southwest | Air | 17398 | 0.857 | -0.383 | 5.499 | 4.290 |
| | | Soil | 17398 | [-0.735, 0.467] | [-5.740, 4.565] | [5.228, 11.948] | [4.317, 9.339] |
| 14 | Northern Brooks Foothills | Air | 8516 | 0.870 | -2.049 | 5.521 | 4.379 |
| | | Soil | 8516 | [-65.715, -2.069] | [-9.454, 1.495] | [3.944, 15.036] | [2.478, 11.427] |
| 15 | North Slope North | Air | 4774 | 0.855 | 1.819 | 6.099 | 4.674 |
| | | Soil | 4774 | [-1.879, -0.409] | [-1.552, 7.579] | [6.976, 10.402] | [6.644, 8.140] |
| 18 | North Slope East | Air | 8880 | 0.895 | 1.040 | 5.176 | 3.987 |
| | | Soil | 8880 | [-1.325, 0.275] | [-6.559, 3.906] | [5.002, 13.198] | [4.124, 9.969] |

## References

Ahajjam, A.: MOREDataset/Alaska-COLD: Alaska-COLDv1.1.0, https://doi.org/10.5281/zenodo.17980272, 2025.

Alaska Center for Conservation Science: Alaska Vegetation and Wetland Composite (AKVWC) [Dataset], https://accscatalog.uaa.alaska.edu/dataset/alaska-vegetation-and-wetland-composite, released 26 November 2017; last modified 16 August 2023. Identifier: a7d0adc9-c495-493f-b0d1-900d7ca74717, 2017.

https://doi.org/10.5194/essd-2026-213
Preprint. Discussion started: 18 May 2026




Biskaborn, B. K., Lanckman, J.-P., Lantuit, H., Elger, K., Streletskiy, D., Cable, W., and Romanovsky, V.: The new database of the Global Terrestrial Network for Permafrost (GTN-P), Earth System Science Data, 7, 245–259, 2015.

Biskaborn, B. K., Smith, S. L., Noetzli, J., Matthes, H., Vieira, G., Streletskiy, D. A., Schoeneich, P., Romanovsky, V. E., Lewkowicz, A. G., Abramov, A., et al.: Permafrost is warming at a global scale, Nature Communications, 10, 264, https://doi.org/10.1038/s41467-018-08240-4, 2019.

Blok, D. et al.: The cooling capacity of mosses: controls on water and energy fluxes in a Siberian tundra site, Ecosystems, 14, 1055–1065, 2011.

Brown, J., Hinkel, K. M., and Nelson, F. E.: The circumpolar active layer monitoring (calm) program: Research designs and initial results[1], Polar Geography, 24, 166–258, https://doi.org/10.1080/10889370009377698, 2000.

Cable, W. L., Romanovsky, V. E., and Jorgenson, M. T.: Scaling-up permafrost thermal measurements in western Alaska using an ecotype approach, The Cryosphere, 10, 2517–2532, 2016.

Campbell Scientific, Inc.: ClimaVue 40 Compact Digital Weather Sensor Product Manual, Logan, UT, revision: 05/2025 edn., available online at https://s.campbellsci.com/documents/us/manuals/climavue40.pdf, 2025.

Campbell Scientific, Inc.: CR350 Measurement and Control Data Logger, https://www.campbellsci.com/cr350, accessed: 16 january 2026, 2026a.

Campbell Scientific, Inc.: SnowVUE10 Digital Ultrasonic Snow Depth Sensor, https://www.campbellsci.com/snowvue10, accessed: 16 January 2026, 2026b.

Cao, B., Gruber, S., Zheng, D., and Li, X.: The ERA5-Land soil temperature bias in permafrost regions, The Cryosphere, 14, 2581–2595, 2020.

Cao, B., Arduini, G., and Zsoter, E.: Brief communication: Improving ERA5-Land soil temperature in permafrost regions using an optimized multi-layer snow scheme, The Cryosphere, 16, 2701–2708, 2022.

Chen, X., Jeong, S., Park, C.-E., Park, H., Joo, J., Chang, D., and Yun, J.: Different responses of surface freeze and thaw phenology changes to warming among Arctic permafrost types, Remote Sensing of Environment, 272, 112 956, 2022.

Chukwuemeka, E.: Electro-Optical and Infrared Aerial Dataset Covering Road Networks & Environment Along Steese Highway, Alaska, Jan 2024, https://doi.org/10.57902/D7GK5Z, 2024.

Chukwuemeka, E., Kreuger, J., and Pasch, T.: Raw Unreviewed Multispectral Imaging Dataset of Roads in Nome, Alaska, Sept. 2022, https://doi.org/10.57902/D7QP4S, 2022a.

Chukwuemeka, E., Kreuger, J., and Pasch, T.: Wind Measurement Dataset Collected with Kestrel Anemometer in Nome, Alaska, Sept. 2022, https://doi.org/10.57902/D7R30Q, 2022b.

Chukwuemeka, E., Kreuger, J., Pasch, T., and Reeder, Z.: High-Resolution Aerial Imagery Dataset for Arctic Transportation Infrastructure Assessment: Steese Highway Corridor, Alaska (August 2023), https://doi.org/10.57902/D7M887, 2023.

Chukwuemeka, E., Keane, S., and Pasch, T.: Field-Based Handheld LiDAR and GNSS Dataset for Arctic Terrain Mapping Along the Dalton Highway (2024), https://doi.org/10.57902/D7BS31, 2024a.

Chukwuemeka, E., Pasch, T., Keane, S., and Kreuger, J.: Arctic Transportation Infrastructure in 3D: High Resolution LiDAR Point Cloud of Road along the Dalton Highway (Chandalar Outhouse–Trevor Creek Area) for Predictive Analytics, August 2024, https://doi.org/10.57902/D7488W, 2024b.

Chukwuemeka, E., Pasch, T., Keane, S., and Kreuger, J.: High-Resolution 3D Point Cloud Representation of a 74-Kilometer Stretch of the Dalton Highway (Toolik Lake–Ice Cut), Alaska, 2024, https://doi.org/10.57902/D70K5M, 2024c.

https://doi.org/10.5194/essd-2026-213
Preprint. Discussion started: 18 May 2026




Chukwuemeka, E., Keane, S., Pasch, T., and Jantzen, J.: Arctic Transportation Infrastructure in 3D: High Resolution LiDAR Point Cloud of Road Segments along the Dalton Highway, Alaska, Winter 2025, https://doi.org/10.57902/D7VS3P, 2025a.

Chukwuemeka, E., Pasch, T., Jantzen, J., and Westphal, W.: Dalton Highway LiDAR Point Cloud Datasets (July 2025): Road Surface and Arctic Infrastructure Mapping, https://doi.org/10.57902/D7N88J, 2025b.

Chukwuemeka, E., Pasch, T., Jantzen, J., and Westphal, W.: High-Resolution Arctic LiDAR Point Cloud Dataset of Road Infrastructure along the Dalton Highway (Trevor–Roche Moutonee), Alaska, for AI-Based Analysis, July 2025, https://doi.org/10.57902/D7830C, 2025c.

Chukwuemeka, E., Pasch, T., Jantzen, J., and Westphal, W.: High-Resolution LiDAR Dataset of the Steese Highway (Eagle Summit to Birch Creek Bridge), Alaska, August 2025, https://doi.org/10.57902/D7HG6M, 2025d.

Chukwuemeka, E., Pasch, T., Jantzen, J., and Westphal, W.: Arctic Geospatial Intelligence: A LiDAR Point Cloud Dataset of Road and Bridge Features along the Steese Highway (Birch Creek) for Machine Learning Applications, Alaska, August 2025, https://doi.org/10.57902/D7CS3B, 2025e.

Clow, G. D.: Temperature data acquired from the DOI/GTN-P Deep Borehole Array on the Arctic Slope of Alaska, 1973–2013, Earth System Science Data, 6, 201–218, 2014.

Cohen, J., Screen, J. A., Furtado, J. C., Barlow, M., Whittleston, D., Coumou, D., Francis, J., Dethloff, K., Entekhabi, D., and Overland, J.: Recent Arctic amplification and extreme mid-latitude weather, Nature geoscience, 7, 627–637, https://www.nature.com/articles/ngeo2234, publisher: Nature Publishing Group UK London, 2014.

Dinerstein, E., Olson, D., Joshi, A., Vynne, C., Burgess, N. D., Wikramanayake, E., Hahn, N., Palminteri, S., Hedao, P., Noss, R., Hansen, M., Locke, H., Ellis, E., Jones, B., Barber, C. V., Hayes, R., Kormos, C., Martin, V., Crist, E., Sechrest, W., Price, L., Baillie, J. E. M., Weeden, D., Suckling, K., Davis, C., Sizer, N., Moore, R., Thau, D., Birch, T., Potapov, P., Turubanova, S., Tyukavina, A., de Souza, N., Pintea, L., Brito, J. C., Llewellyn, O. A., Miller, A., Patzelt, A., Ghazanfar, S. A., Timberlake, J., Klöser, H., Shennan-Farpón, Y., Kindt, R., Lillesø, J.-P. B., van Breugel, P., Graudal, L., Voge, M., Al-Shammari, K. F., and Saleem, M.: An Ecoregion-Based Approach to Protecting Half the Terrestrial Realm, BioScience, 67, 534–545, https://doi.org/10.1093/biosci/bix014, 2017.

Hengl, T.: Sand content in % (kg / kg) at 6 standard depths (0, 10, 30, 60, 100 and 200 cm) at 250 m resolution [Dataset], https://doi.org/10.5281/zenodo.2525662, 2018.

Hengl, T. and MacMillan, R. A.: Predictive soil mapping with R, OpenGeoHub Foundation: Wageningen, The Netherlands, 370, 2019.

Herrington, T. C., Fletcher, C. G., and Kropp, H.: Validation of pan-Arctic soil temperatures in modern reanalysis and data assimilation systems, The Cryosphere, 18, 1835–1861, https://doi.org/10.5194/tc-18-1835-2024, 2024.

Hjort, J., Streletskiy, D., Doré, G., Wu, Q., Bjella, K., and Luoto, M.: Impacts of permafrost degradation on infrastructure, Nature Reviews Earth & Environment, 3, 24–38, https://www.nature.com/articles/s43017-021-00247-8, publisher: Nature Publishing Group UK London, 2022.

Jorgenson, M., Yoshikawa, K., Kanevskiy, M., Shur, Y., Romanovsky, V., Marchenko, S., Grosse, G., Brown, J., and Jones, B.: Permafrost characteristics of Alaska, 2008.

Karevan, Z. and Suykens, J. A.: Transductive feature selection using clustering-based sample entropy for temperature prediction in weather forecasting, Entropy, 20, 264, 2018.

Karunaratne, K. and Burn, C.: Freezing n-factors in discontinuous permafrost terrain, Takhini River, Yukon Territory, Canada, in: Proceedings of the 8th International Conference on Permafrost, vol. 1, pp. 519–524, University of Alaska: Fairbanks, 2003.

Klene, A. E., Nelson, F. E., Shiklomanov, N. I., and Hinkel, K. M.: The n-factor in natural landscapes: variability of air and soil-surface temperatures, Kuparuk River Basin, Alaska, USA, Arctic, Antarctic, and Alpine Research, 33, 140–148, 2001.

https://doi.org/10.5194/essd-2026-213
Preprint. Discussion started: 18 May 2026




Kurylyk, B. L., Hayashi, M., Quinton, W. L., McKenzie, J. M., and Voss, C. I.: Influence of vertical and lateral heat transfer on permafrost thaw, peatland landscape transition, and groundwater flow, Water Resources Research, 52, 1286–1305, 2016.

Manos, E., Witharana, C., and Liljedahl, A. K.: Permafrost thaw-related infrastructure damage costs in Alaska are projected to double under medium and high emission scenarios, Communications Earth & Environment, 6, 221, https://doi.org/10.1038/s43247-025-02191-7, publisher: Nature Publishing Group, 2025.

Muñoz Sabater, J. n., Dutra, E., Agustí-Panareda, A., Albergel, C., Arduini, G., Balsamo, G., Boussetta, S., Choulga, M., Harrigan, S., Hersbach, H., Martens, B., Miralles, D. G., Piles, M. a., Rodrí guez Fernández, N. J., Zsoter, E., Buontempo, C., and Thépaut, J.-N.: ERA5-Land: A State-of-the-art Global Reanalysis Dataset for Land Applications [Dataset], https://doi.org/10.5194/essd-13-4349-2021, 2021.

Onset Computer Corporation: HOBO H21-USB Weather Station, https://www.onsetcomp.com/products/data-loggers/h21-usb, accessed: 16 january 2026, 2026a.

Onset Computer Corporation: HOBO U30 USB Weather Station, https://www.onsetcomp.com/products/data-loggers/u30-nrc, accessed: 16 january 2026, 2026b.

Onset Computer Corporation: S-TMB-M002 12-Bit Temperature Smart Sensor, https://www.onsetcomp.com/products/sensors/s-tmb-m0xx, accessed: 16 january 2026, 2026c.

Osterkamp, T. E.: The recent warming of permafrost in Alaska, Global and Planetary Change, 49, 187–202, 2005.

Park, H., Kim, Y., and Kimball, J. S.: Widespread permafrost vulnerability and soil active layer increases over the high northern latitudes inferred from satellite remote sensing and process model assessments, Remote Sensing of Environment, 175, 349–358, https://doi.org/10.1016/j.rse.2015.12.046, 2016.

Pasch, T., Chukwuemeka, E., and Krueger, J.: High Resolution LiDAR data covering road networks in Nome, Alaska – Site 1, https://doi.org/10.57902/D74W2T, 2023a.

Pasch, T., Chukwuemeka, E., and Krueger, J.: High Resolution LiDAR data covering road networks in Nome, Alaska – Site 2, https://doi.org/10.57902/D71599, 2023b.

Pasch, T., Chukwuemeka, E., and Krueger, J.: High Resolution LiDAR data covering road networks in Nome, Alaska – Site 3, https://doi.org/10.57902/D7WC7C, 2023c.

Pasch, T., Chukwuemeka, E., and Krueger, J.: High Resolution LiDAR data covering road networks in Nome, Alaska – Site 4, https://doi.org/10.57902/D7RP43, 2023d.

Pasch, T., Chukwuemeka, E., and Krueger, J.: High Resolution LiDAR data covering road networks in Nome, Alaska – Site 5, https://doi.org/10.57902/D7MW25, 2023e.

Pasch, T., Chukwuemeka, E., and Krueger, J.: High Resolution LiDAR data covering road networks in Nome, Alaska – Site 6, https://doi.org/10.57902/D7H59N, 2023f.

Pasch, T., Chukwuemeka, E., and Krueger, J.: High Resolution LiDAR data covering road networks in Nome, Alaska – Site 7, https://doi.org/10.57902/D7CC7Q, 2023g.

Pasch, T., Chukwuemeka, E., and Krueger, J.: High Resolution LiDAR data covering road networks in Nome, Alaska – Site 8, https://doi.org/10.57902/D77P4F, 2023h.

Pasch, T., Chukwuemeka, E., and Krueger, J.: High Resolution LiDAR data covering road networks in Nome, Alaska – Site V_1, https://doi.org/10.57902/D73W2H, 2023i.

https://doi.org/10.5194/essd-2026-213
Preprint. Discussion started: 18 May 2026




Pasch, T., Chukwuemeka, E., and Krueger, J.: High Resolution LiDAR data covering road networks in Nome, Alaska – Site V_2, https://doi.org/10.57902/D70590, 2023j.

Pasch, T. J. and UND ARCTIC Lab: UND ARCTIC Lab: Defense Resiliency Platform Against Extreme Cold Weather, https://arts-sciences.und.edu/academics/communication/arctic/index.html, university of North Dakota, Department of Communication. Accessed: 2025-11-21, 2024.

Pincus, S. M. and Goldberger, A. L.: Physiological time-series analysis: what does regularity quantify?, American Journal of Physiology-Heart and Circulatory Physiology, 266, H1643–H1656, 1994.

Porada, P., Ekici, A., and Beer, C.: Effects of bryophyte and lichen cover on permafrost soil temperature at large scale, The Cryosphere, 10, 2291–2315, https://doi.org/10.5194/tc-10-2291-2016, 2016.

Porter, C. and et al.: ArcticDEM, Version 4.1 [Dataset], https://doi.org/10.7910/DVN/3VDC4W, accessed 10/17/2025, 2023.

Putkonen, J.: Soil thermal processes and heat transfer processes near Ny-Ålesund, northwestern Spitsbergen, Svalbard, Polar research, 17, 165–179, 1998.

Rantanen, M., Karpechko, A. Y., Lipponen, A., Nordling, K., Hyvärinen, O., Ruosteenoja, K., Vihma, T., and Laaksonen, A.: The Arctic has warmed nearly four times faster than the globe since 1979, Communications earth & environment, 3, 168, 2022.

Romanovsky, V. and Osterkamp, T.: Interannual variations of the thermal regime of the active layer and near-surface permafrost in northern Alaska, Permafrost and Periglacial Processes, 6, 313–335, 1995.

Romanovsky, V. E., Drozdov, D. S., Oberman, N. G., Malkova, G. V., Kholodov, A. L., Marchenko, S. S., Moskalenko, N. G., Sergeev, D. O., Ukraintseva, N. G., Abramov, A. A., et al.: Thermal state of permafrost in Russia, Permafrost and Periglacial Processes, 21, 136–155, 2010a.

Romanovsky, V. E., Smith, S. L., and Christiansen, H. H.: Permafrost thermal state in the polar Northern Hemisphere during the international polar year 2007–2009: a synthesis, Permafrost and Periglacial processes, 21, 106–116, 2010b.

Smith, S. L., O'Neill, H. B., Isaksen, K., Noetzli, J., and Romanovsky, V. E.: The changing thermal state of permafrost, Nature Reviews Earth & Environment, 3, 10–23, 2022.

Steinhart, J. S. and Hart, S. R.: Calibration curves for thermistors, in: Deep sea research and oceanographic abstracts, vol. 15, pp. 497–503, Elsevier, 1968.

Streletskiy, D., Maslakov, A., Noetzli, J., Schoeneich, P., Smith, S. L., Vieira, G., and Irrgang, A.: Sustaining permafrost observations: priorities and needs of the Global Terrestrial Network for Permafrost (GTN-P), Arctic Observing Summit 2020 White Paper, 2020.

Stuenzi, S. M., Boike, J., Cable, W., Herzschuh, U., Kruse, S., Pestryakova, L. A., Schneider von Deimling, T., Westermann, S., Zakharov, E. S., and Langer, M.: Sensitivity of ecosystem-protected permafrost under changing boreal forest structures, Environmental Research Letters, 16, 084 045, https://doi.org/10.1088/1748-9326/ac153d, 2021.

Swanson, D. K., Sousanes, P. J., and Hill, K.: Increased mean annual temperatures in 2014–2019 indicate permafrost thaw in Alaskan national parks, Arctic, Antarctic, and Alpine Research, 53, 1–19, 2021.

Urban, F. E. and Clow, G. D.: DOI/GTN-P climate and active-layer data acquired in the National Petroleum Reserve-Alaska and the Arctic National Wildlife Refuge, 1998-2019, Tech. rep., US Geological Survey, 2018.

U.S. Army Corps of Engineers Cold Regions Research and Engineering Laboratory: Defense Resiliency Platform (DRP), https://drp.dataone.org/, accessed: 2025-11-21, 2024.

Walsh, J. E. and Brettschneider, B.: Attribution of recent warming in Alaska, Polar Science, 21, 101–109, 2019.

https://doi.org/10.5194/essd-2026-213
Preprint. Discussion started: 18 May 2026




Wang, K., Jafarov, E., Overeem, I., Romanovsky, V., Schaefer, K., Clow, G., Urban, F., Cable, W., Piper, M., Schwalm, C., Zhang, T., Kholodov, A., Sousanes, P., Loso, M., and Hill, K.: A synthesis dataset of permafrost-affected soil thermal conditions for Alaska, USA, Earth System Science Data, 10, 2311–2328, https://doi.org/10.5194/essd-10-2311-2018, publisher: Copernicus GmbH, 2018.

Zanaga, D., Van De Kerchove, R., Daems, D., De Keersmaecker, W., Brockmann, C., Kirches, G., Wevers, J., Cartus, O., Santoro, M., Fritz, S., Lesiv, M., Herold, M., Tsendbazar, N.-E., Xu, P., Ramoino, F., and Arino, O.: ESA WorldCover 10 m 2021 v200 [Dataset], https://doi.org/10.5281/zenodo.7254221, 2022.

Zhang, T., Frauenfeld, O. W., Serreze, M. C., Etringer, A., Oelke, C., McCreight, J., Barry, R. G., Gilichinsky, D., Yang, D., and Ye, H.: Spatial and temporal variability in active layer thickness over the Russian Arctic drainage basin, Journal of Geophysical Research: Atmospheres, 110, D16 101, https://doi.org/10.1029/2004JD005642, 2005.

Zhao, Y., Natali, S. M., Rogers, B. M., Watts, J. D., Mack, M. C., Perron, J. T., and Raciti, S. M.: Canopy-mediated climate feedbacks in the boreal continuous permafrost zone, Research Square preprint, https://doi.org/10.21203/rs.3.rs-7961174/v1, preprint, 2025.